

# ZnO Nanostructures for Dye-Sensitized Solar Cells

By Qifeng Zhang,\* Christopher S. Dandeneau, Xiaoyuan Zhou, and Guozhong Cao\*

This Review focuses on recent developments in the use of ZnO nanostructures for dye-sensitized solar cell (DSC) applications. It is shown that carefully designed and fabricated nanostructured ZnO films are advantageous for use as a DSC photoelectrode as they offer larger surface areas than bulk film material, direct electron pathways, or effective light-scattering centers, and, when combined with TiO<sub>2</sub>, produce a core-shell structure that reduces the combination rate. The limitations of ZnO-based DSCs are also discussed and several possible methods are proposed so as to expand the knowledge of ZnO to TiO<sub>2</sub>, motivating further improvement in the power-conversion efficiency of DSCs.

crystalline silicon semiconductor can reach 92% of the theoretical attainable energy conversion, with 20% conversion efficiency in commercial designs. However, because of the considerably high material costs, thin-film solar cells have been developed to address the product costs.<sup>[8–10]</sup> Amorphous silicon ( $\alpha$ -Si) is a candidate for thin-film solar cells because its defect energy level can be controlled by hydrogenation and the band gap can be reduced so that the light-absorption efficiency is much higher than crystalline silicon.<sup>[11,12]</sup> The problem is that amorphous silicon tends to be unstable and can lose up to 50% of its efficiency

## 1. Introduction

The increasing demand for fossil fuels and the environmental impact of their use are continuing to exert pressure on an already-stretched world energy infrastructure. Significant progress has been made in the development of renewable-energy technologies, such as solar cells, fuel cells, and biofuels. However, although these alternative energy sources have been marginalized in the past, it is expected that new technology could make them more practical and price competitive with fossil fuels, thus enabling an eventual transition away from fossil fuels as our primary energy sources. Solar energy is considered to be the ultimate solution to the energy and environmental challenge as a carbon-neutral energy source.

The conversion from solar energy to electricity is fulfilled by solar-cell devices based on the photovoltaic effect. Many photovoltaic devices have already been developed over the past five decades.<sup>[1–3]</sup> However, wide-spread use is still limited by two significant challenges, namely conversion efficiency and cost.<sup>[4–6]</sup> One of the traditional photovoltaic devices is the single-crystalline silicon solar cell, which was invented more than 50 years ago and currently makes up 94% of the market.<sup>[7]</sup> Single-crystalline silicon solar cells operate on the principle of p–n junctions formed by joining p-type and n-type semiconductors. The electrons and holes are photogenerated at the interface of p–n junctions, separated by the electrical field across the p–n junction, and collected through external circuits. In principle, the single-

within the first hundred hours. Today, commercial roof products are available that operate at  $\approx 15\%$  efficiency. Bridging the gap between single-crystalline silicon and amorphous silicon is the polycrystalline-silicon film, for which a conversion efficiency of around 18% is obtained.<sup>[13–15]</sup> Compound semiconductors, such as gallium arsenide (GaAs), cadmium telluride (CdTe), and copper indium gallium selenide (CIGS), receive much attention because they present direct energy gaps, can be doped to either p-type or n-type, have band gaps matching the solar spectrum, and have high optical absorbance.<sup>[16–18]</sup> These devices have demonstrated single-junction conversion efficiencies of 16–32%.<sup>[19]</sup> Although those photovoltaic devices built on silicon or compound semiconductors have been achieving high efficiency for practical use, they still require major breakthroughs to meet the long-term goal of very-low cost ( $\text{US}\$0.40 \text{ kWh}^{-1}$ ).<sup>[1]</sup>

To aim at further lowering the production costs, dye-sensitized solar cells (DSCs) based on oxide semiconductors and organic dyes or metallorganic-complex dyes have recently emerged as promising approach to efficient solar-energy conversion. The DSCs are a photoelectrochemical system, which incorporate a porous-structured oxide film with adsorbed dye molecules as the photosensitized anode. A platinized fluorine-doped tin oxide (FTO) glass acts as the counter electrode (i.e., cathode), and a liquid electrolyte that traditionally contains  $\text{I}^-/\text{I}_3^-$  redox couples serves as a conductor to electrically connect the two electrodes.<sup>[20–25]</sup> During operation, photons captured by the dye monolayer create excitons that are rapidly split at the nanocrystallite surface of the oxide film. Electrons are injected into the oxide film and holes are released by the redox couples in the liquid electrolyte (Fig. 1a). Compared with the conventional single-crystal silicon-based or compound-semiconductor thin-film solar cells, DSCs are thought to be advantageous as a photovoltaic device possessing both practicable high efficiency and cost effectiveness. To date, the most successful DSC was obtained on

[\*] Dr. Q. F. Zhang, C. S. Dandeneau, Dr. X. Y. Zhou, Prof. G. Z. Cao  
Department of Materials Science and Engineering  
University of Washington, Seattle, WA 98195 (USA)  
E-mail: qfzhang@u.washington.edu; gzcao@u.washington.edu

DOI: 10.1002/adma.200803827

TiO<sub>2</sub> nanocrystalline film (Fig. 1b) combined with a ruthenium–polypyridine complex dye, as first reported by O’Regan and Grätzel in 1991.<sup>[26]</sup> Following this idea, a certified overall conversion efficiency of 10.4% was achieved on a TiO<sub>2</sub>–RuL(NCS)<sub>3</sub> (“black dye”) system, in which the spectral response of the complex dye was extended into the near-infrared region so as to absorb far more of the incident light.<sup>[20,27–29]</sup> The porous nature of nanocrystalline TiO<sub>2</sub> films drives their use in DSCs due to the large surface area available for dye-molecule adsorption. Meanwhile, the suitable relative energy levels at the semiconductor–sensitizer interface (i.e., the position of the conduction-band edge of TiO<sub>2</sub> being lower than the excited-state energy level of the dye) allow for the effective injection of electrons from the dye molecules to the semiconductor.<sup>[30]</sup>

The achievement of acceptable conversion efficiency puts great confidence in the ability of DSCs to challenge the high cost of commercially available solar cells based on silicon or compound semiconductors. However, a further increase in conversion efficiency has been limited by energy loss due to recombination between electrons and either the oxidized dye molecules or electron-accepting species in the electrolyte during the charge-transport process.<sup>[31–33]</sup> Such a recombination is predominately derived from the lack of a depletion layer on the TiO<sub>2</sub> nanocrystallite surface, and becomes significantly serious when the thickness of the photoelectrode film is increased. To understand this issue, DSC technology based on ZnO has been explored extensively. ZnO is a wide-band-gap semiconductor that possesses an energy-band structure and physical properties similar to those of TiO<sub>2</sub> (Table 1), but has higher electronic mobility that would be favorable for electron transport, with reduced recombination loss when used in DSCs. Many studies have already been reported on the use of ZnO material for application in DSCs. Although the conversion efficiencies of 0.4–5.8% obtained for ZnO are much lower than that of 11% for TiO<sub>2</sub>, ZnO is still thought of as a distinguished alternative to TiO<sub>2</sub> due to its ease of crystallization and anisotropic growth. These properties allow ZnO to be produced in a wide variety of nanostructures, thus presenting unique properties for electronics, optics, or photocatalysis.<sup>[34–41]</sup> In particular, recent studies



**Qifeng Zhang** received his Ph. D. degree from Peking University (China) in 2001. He is currently working in University of Washington as an Acting Assistant Professor-Temp. His research interests involve engineering applications of nanostructured materials on electrical devices including solar cells, UV light-emitting diodes (LEDs), field-effect transistors (FETs), and gas sensors.



**Guozhong Cao** is Boeing-Steiner Professor of Materials Science and Engineering and Adjunct Professor of Chemical and Mechanical Engineering at the University of Washington. He has published over 200 refereed papers, and authored and edited 4 books including “Nanostructures and Nanomaterials”. His current research is focused mainly on nanomaterials for energy conversion and storage, including solar cells, lithium-ion batteries, supercapacitors, and hydrogen-storage materials.

on ZnO-nanostructure-based DSCs have delivered many new concepts, leading to a better understanding of photoelectrochemically based energy conversion. This, in turn, would speed up the development of DSCs that are associated with TiO<sub>2</sub>.

One of the defining features of nanostructures is their basic units on the nanometer scale. This, first of all, provides the nanostructures with a large specific surface area. It may also

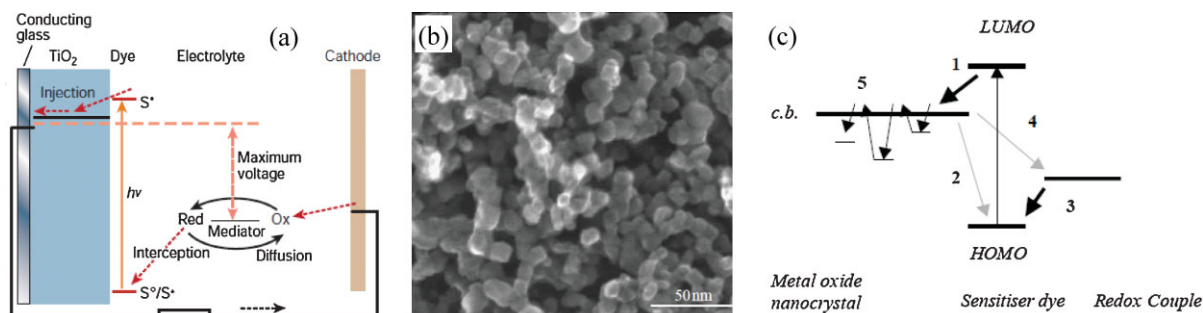


**Figure 1.** A dye-sensitized solar cell based on an electrochemical system. a) Schematic of the construction and operational principle of the device. Reproduced with permission from [20]. Copyright 2001, Macmillan Magazines Ltd. b) SEM image of an oxide (TiO<sub>2</sub>) electrode film with nanocrystallites ( $\approx 20$  nm in diameter). Reproduced with permission from [29]. Copyright 2007, The Royal Society. c) Electron transport in nanocrystalline oxide electrodes, in which photoexcited electrons are injected from the dye to the conduction band (denoted as “c.b.”) of the nanocrystallite (1), the dye is regenerated by electron transfer from a redox couple in the electrolyte (3), and a recombination may take place between the injected electrons and the dye cation (2) or redox couple (4). The latter (4) is normally believed to be the predominant loss mechanism. Electron trapping in the nanocrystallites (5) is also a mechanism that causes energy loss. LUMO and HOMO represent the lowest unoccupied molecular orbital and the highest occupied molecular orbital of the dye, respectively. Reproduced with permission from [30]. Copyright 2004, Elsevier.

**Table 1.** A comparison of physical properties of ZnO and TiO<sub>2</sub>.

	ZnO	TiO <sub>2</sub>	Reference
Crystal structure	rocksalt, zinc blende, and wurtzite	rutile, anatase, and brookite	[42,43]
Energy band gap [eV]	3.2–3.3	3.0–3.2	[42–44]
Electron mobility [cm <sup>2</sup> V s <sup>-1</sup> ]	205–300 (bulk ZnO), 1000 (single nanowire)	0.1–4	[42,43,45]
Refractive index	2.0	2.5	[46]
Electron effective mass [ <i>m<sub>e</sub></i> ]	0.26	9	[44]
Relative dielectric constant	8.5	170	[44]
Electron diffusion coefficient [cm <sup>2</sup> s <sup>-1</sup> ]	5.2 (bulk ZnO), 1.7 × 10 <sup>-4</sup> (nanoparticulate film)	0.5 (bulk TiO <sub>2</sub> ), ≈10 <sup>-8</sup> –10 <sup>-4</sup> (nanoparticulate film)	[47,48]

result in many particular behaviors in electron transport or light propagation in view of the surface effect, quantum-confinement effect, or photon localization.<sup>[49–51]</sup> Those nanostructural forms of ZnO developed during the past several decades mainly include nanoparticles,<sup>[52,53]</sup> nanowires (or nanorods),<sup>[54,55]</sup> nanotubes,<sup>[56]</sup> nanobelts,<sup>[57]</sup> nanosheets,<sup>[54,58]</sup> and nanotips.<sup>[34,38]</sup> The production of these structures can be achieved through sol–gel synthesis,<sup>[53]</sup> hydrothermal/solvothermal growth,<sup>[54]</sup> physical or chemical vapor deposition,<sup>[55,57]</sup> low-temperature aqueous growth,<sup>[56,59]</sup> chemical bath deposition,<sup>[60]</sup> or electrochemical deposition.<sup>[58,61,62]</sup> In this article, recent developments in ZnO nanostructures, particularly for application in DSCs, are reviewed. It will show that photoelectrode films with nanostructured ZnO can significantly enhance solar-cell performance by offering a large surface area for dye adsorption, direct transport pathways for photoexcited electrons, and efficient scattering centers for enhanced light-harvesting efficiency. In addition, ZnO may be combined with TiO<sub>2</sub> via a core–shell structure for reduced combination rates. The limitations of ZnO-based DSCs are also discussed. In the final section, several attempts to expand ZnO concepts to TiO<sub>2</sub> are presented to motivate further improvement in the conversion efficiency of DSCs.

## 2. Nanostructures Offering Large Specific Surface Area

A large internal surface area is the foremost requirement of the photoelectrode film in DSCs, so that sufficient dye molecules can be adsorbed to act as an “antenna” for the capture of incident photons. Nanomaterials can satisfy this requirement due to the formation of a porous interconnected network in which the specific surface area may be increased by more than 1000 times when compared with bulk materials.<sup>[63]</sup> The abundant forms of ZnO nanostructures provide a great deal of opportunities to obtain high surface-area-to-volume ratios, which in turn contribute to dye adsorption, as well as light harvesting, in DSCs.

### 2.1. ZnO Nanoparticulate Films

ZnO films with nanoparticles for application in DSCs have been extensively studied, partially due to the direct availability of porous structures with assembled nanoparticles and the simplicity of synthesis of nanoparticles via chemically based solution methods. Due to the mechanism of charge transfer between the dye and semiconductor, the strategy for studying DSCs with nanoparticulate ZnO films is almost the same as that adopted for

nanocrystalline TiO<sub>2</sub>. It can be somewhat regarded as a straight implantation of TiO<sub>2</sub>-based Grätzel-type solar-cell technology, in which the TiO<sub>2</sub> nanoparticles are replaced by ZnO nanoparticles while the dye sensitizer and the electrolyte remain unchanged.

#### 2.1.1. Sol–Gel Derived Nanocrystalline Films

A traditional method of synthesizing ZnO nanoparticles is achieved by the preparation of ZnO sols in the liquid phase from homogeneous ethanolic solutions with precursors of lithium hydroxide and zinc acetate.<sup>[64–66]</sup> The resulting sol contains ZnO nanoparticles with an average diameter ranging from ten to several tens of nanometers. A further process is performed on the sol to yield film by spin coating or dip coating, during which the system is converted from liquid sol into solid wet gel. Following drying and heat treatment, the gel is thermalized so as to generate a porous structured film on the substrate. The doctor-blade method<sup>[67,68]</sup> is also a frequently adopted approach for the preparation of ZnO nanocrystalline film, during which Triton X-100 (1% by volume) is conventionally added to the sol to facilitate the film formation. Residual organics are removed by a subsequent heat treatment, typically at temperatures between 300 °C and 400 °C. For DSC applications, the film is sensitized by immersion in ruthenium–polypyridine-complex dyes (so-called N3, N719, or black dye that is commercially available) for a given amount of time.<sup>[69–71]</sup> For use as working electrode, the as-sensitized film is constructed to a cell device by assembling it with a counter electrode consisting of a thin platinum layer deposited on FTO glass. An electrolyte solution containing KI (0.5 M) and I<sub>2</sub> (0.03 M) in a mixed solvent with ethylene carbonate and acetonitrile (60%:40% by volume) is then introduced to the interval of the two electrodes. The performance of the solar cell is characterized by recording the current–voltage (*I*–*V*) behavior when the cell is irradiated under AM 1.5-type simulated sunlight. The overall power conversion efficiency,  $\eta$ , can be calculated according to

$$\eta = \frac{FF \times V_{OC} \times I_{SC}}{P_{in}} \quad (1)$$

and the fill factor (*FF*) is defined as

$$FF = \frac{V_{max} \times I_{max}}{V_{OC} \times I_{SC}} \quad (2)$$

where *P<sub>in</sub>* is the input power density (i.e., the intensity of incident light, in mW cm<sup>-2</sup>), *V<sub>OC</sub>* is the open-circuit voltage (mV), *I<sub>SC</sub>* is the short-circuit current density (mA cm<sup>-2</sup>), and *V<sub>max</sub>* and *I<sub>max</sub>*

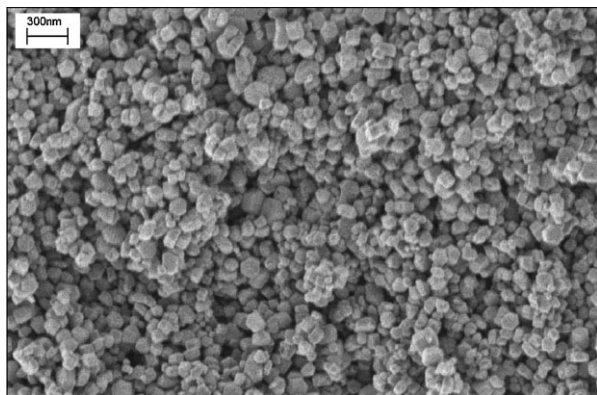


**Figure 2.** SEM image of a ZnO-nanoparticle electrode prepared with a compression method. Reproduced with permission from [73]. Copyright 2002, Elsevier.

are the voltage and current at maximum power output, respectively.

At the early developmental stage, using sol-gel-derived ZnO-nanoparticle films, the reported conversion efficiencies of DSCs are fairly low, with values generally around 0.4–2.22%.<sup>[66,67,72]</sup> The scattered distribution of efficiencies implies that the solar-cell performance is sensitive to many factors, including the size and shape of the nanoparticles, the porosity of film, the film-fabrication technique, and the post-treatment of the photoelectrode.

With regard to the improvement of conversion efficiency in ZnO DSCs, Keis et al. reported a compression method for the film fabrication to achieve a highly active ZnO surface for dye adsorption.<sup>[73,74]</sup> In this process, ZnO nanoparticles with an average size of  $\approx 150$  nm (Fig. 2) were synthesized via a sol-gel route, and, in particular, the film was prepared by compressing the nanoparticle powder under a pressure of  $1000 \text{ kg cm}^{-2}$ . When the obtained film was used in a DSC under illumination with an intensity of  $10 \text{ mW cm}^{-2}$ , an overall conversion efficiency as high as 5% was achieved.<sup>[73–75]</sup> Comparing this result with the 2–2.1% conversion efficiencies attained for ZnO films with 150-nm nanoparticles prepared using the aforementioned doctor-blade method without compression,<sup>[76,77]</sup> the authors explained that the improvement in solar-cell performance was due to the increased interfacial kinetics inherent in the compression method that didn't involve a heat-treatment process. It had been demonstrated that such increased interfacial kinetics could result in a more efficient injection of electrons from the dye molecules to the ZnO semiconductor. In this work, although the light-scattering effect is not addressed as a significant reason promoting the light harvesting, it is likely that ZnO nanoparticles with sizes of  $\approx 150$  nm play a role in the generation of light scattering, leading to additional contribution to the light harvest.

### 2.1.2. Electrostatic Spray Deposition Technique for Nanoparticulate Films

Highly efficient conversion can be also obtained for nanoparticulate-ZnO films fabricated by using an electrostatic spray deposition (ESD) technique developed by Jansen et al. for coating

electrode films.<sup>[78,79]</sup> The basic principle of ESD is the generation of an aerosol using organic solvents containing inorganic or organometallic precursors under the influence of a high voltage. An aerosol is defined as a dispersion of solid particles or liquid droplets in a gaseous ambient. In order to obtain such an aerosol of micrometer-sized droplets, the precursor liquid is pumped through a metal nozzle. Usually a spherical droplet is formed at the tip of the nozzle, but if a high voltage is applied (typically 6–15 kV) between the nozzle and a grounded substrate, this droplet at the tip of the nozzle transforms into a conical shape and fans out to form a spray of highly charged droplets. The generated spray droplets are attracted by the grounded and heated substrate as a result of the applied potential difference. Consequently, the droplets impinge on the heated substrate, where they lose their charge. After complete solvent evaporation, a thin layer consisting of the inorganic product is left on the substrate surface.<sup>[78]</sup> The advantages of the ESD technique are (1) the great variety of tailored film morphologies, (2) the possibility of controlling the chemical composition of the deposited coatings, and (3) the high deposition efficiency, since the electric field directs the charged droplets to the substrate.

As for a typical preparation of nanoparticulate ZnO films with the ESD technique,<sup>[80]</sup> a colloidal solution of precursor was prepared through the hydrolysis of zinc salts in the presence of an amine and then mixed with polyvinyl alcohol (PVA) that was dissolved in a mixture of ethanol and water. The nanoparticle-containing precursor solution thus obtained was subsequently used for the ESD deposition of ZnO film. PVA was employed to prevent the agglomeration of ZnO during the high-temperature calcination process. With this fabrication, both the porosity and the specific surface area of the films can be controlled by adjusting the weight ratio of nanoparticles to PVA. It has been reported that a ratio of 1.8 may yield a maximum specific surface area of  $12.55 \text{ m}^2 \text{ g}^{-1}$  and a peak photovoltaic efficiency of 3.4%. Recently, this technique was also exploited in the synthesis of  $\text{TiO}_2$  nanofibers, achieving an overall conversion efficiency of around 5%.<sup>[81,82]</sup>

## 2.2. Nanoporous Structured ZnO Films

Besides nanoparticulate films, nanoporous structured ZnO films were also studied as photoelectrodes in DSCs due to their high porosity. Many techniques have been reported for the preparation of nanoporous ZnO films.<sup>[61,62,83,84]</sup> Among these methods, electrochemical deposition and chemical bath deposition show characteristics advantageous to forming nanoporous films with nanowalls vertically grown on the substrate. Such a structure is thought to be favorable for electron transport from the point of generation to the collection electrode in DSCs and, also, favorable for electrolyte diffusion through the intervals between the nanowalls, resulting in a decrease in both the series resistance and recombination rate of the cell.

### 2.2.1. Electrochemical Deposition Fabrication

Electrochemical deposition is a simple and low-cost route for the preparation of nanoporous films possessing a large surface area. The advantage of this method is that the growth orientation, morphology, and thickness of the films can be modestly

controlled by adjusting the deposition parameters (deposition voltage, current density, temperature, etc.). A typical fabrication process for the electrochemical deposition of nanoporous ZnO films at low temperature was described by Xi et al.<sup>[61]</sup> In this fabrication, a two-electrode system was used, consisting of a Zn sheet as the anode and glass coated with indium tin oxide (ITO) as the cathode. The electrolyte contained 0.04 M zinc nitrate and 0.04 M hexamethyleneteramine (HMT) in a solvent formed by a mixture of distilled water and ethanol with a volume ratio of 1 to 1. HMT was employed in the electrolyte as a buffer to obtain a pH value of around 6. The additional ethanol in the electrolyte acted as a wetting agent to improve the thickness uniformity and surface coverage. The deposition of porous ZnO films was carried out at 40 °C in a water bath with a bias voltage of 0.5–0.7 V. It was demonstrated that, in the case of an applied voltage of 0.5 V only, the obtained films presented a sheet-like morphology and, under high scanning electron microscopy (SEM) magnification, the films were observed to comprise of pellet-like polycrystalline particles of about 250 nm in diameter (20–30 nm grain size). These particles were interconnected with pore sizes ranging from 500 nm to 2 μm (Fig. 3a). Other applied voltages produced films with a more irregular porous structure. The as-deposited film thickness is correlated to both the bias voltage and the deposition time. Typically, a thickness of about 2.6 μm can be obtained at 0.5 V for 30 min, 2.4 μm at 0.7 V for 20 min, and 3.4 μm at 0.7 V for 30 min. The temperature of the water bath also shows an influence on the film structure. Increasing the temperature to 70 °C would result in a ZnO film with a compact structure, showing a much lower photovoltaic efficiency than the porous film due to the decreased internal surface area.

In electrochemical deposition, the nucleation rate can significantly affect the film structure, especially in terms of the porosity. Through the use of a surfactant to mediate the nucleation, ZnO films with a more porous structure have been developed for DSC application. Poly (vinyl pyrrolidone) (PVP) was reported as a highly efficient surfactant that had been combined with the electrochemical deposition method to produce nanoporous ZnO films with very impressive photovoltaic efficiencies.<sup>[85]</sup> It was demonstrated that as-obtained films possessed a structure comprised of interconnected crystal grains. The grain size, and thus the surface morphology of ZnO films, could be strongly influenced by the PVP concentration. That is, increased PVP concentration would result in a reduced grain size. Typically, when the PVP concentration was 4 g L<sup>-1</sup>, the grain size was

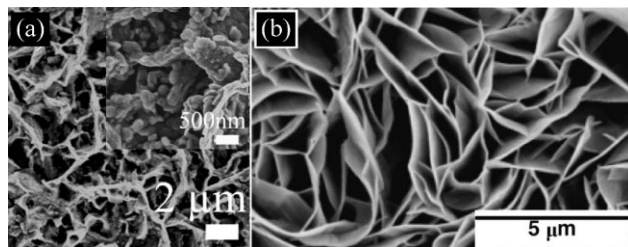


**Figure 3.** SEM images of nanoporous ZnO films. a) Electrochemically deposited film without using reagent. Reproduced with permission from [61]. Copyright 2008, The Electrochemical Society. b) Chemical-bath-deposited nest-like ZnO film. Reproduced with permission from [89]. Copyright 2003, Elsevier.

reduced to 20–40 nm. However, no ZnO film could be formed if the concentration was larger than 6 g L<sup>-1</sup>. The DSCs with ZnO films synthesized by this method exhibit an extremely high conversion efficiency of 5.08% under 53 mW cm<sup>-2</sup> illumination, while the photoelectrode consists of electrochemically deposited double-layer ZnO films, typically containing 8-μm-thick nanoporous film on a 200-nm-thick compact nanocrystalline film.

### 2.2.2. Chemical Bath Deposition Fabrication

Chemical bath deposition (CBD), developed for producing ceramic films from aqueous solutions at low temperatures by pyrolysis of layered metal hydroxides, has also been used for the fabrication of nanoporous ZnO films.<sup>[86,87]</sup> A typical process for this fabrication can be described in the following steps: (1) the formation of layered basic zinc acetate (LBZA), Zn<sub>5</sub>(OH)<sub>8</sub>(CH<sub>3</sub>COO)<sub>2</sub>·2H<sub>2</sub>O, by hydrolysis of zinc acetate dihydrate in methanol, (2) the deposition of the LBZA film on a substrate at 60 °C through heterogeneous nucleation, and (3) a heat treatment at a temperature above 150 °C so as to transform the LBZA film into crystalline ZnO. A similar method was also reported for the formation of nanoporous ZnO films via layered hydroxide zinc carbonate (LHZC) using a solution of zinc nitrate hexahydrate and urea in water.<sup>[88]</sup> Films synthesized through this method show a nest-like morphology and porous structure (Fig. 3b).<sup>[89]</sup> Studies in greater detail pointed out that films fabricated by CBD were composed of sheet-like grains with ≈11 nm ZnO crystallites, pore sizes of ≈12 nm, and surface areas of about 25 m<sup>2</sup> g<sup>-1</sup>.<sup>[90,91]</sup>

Hosono et al.<sup>[88,89,92]</sup> systematically studied the DSC performance of nanoporous structured ZnO films fabricated by the CBD technique. They achieved an overall conversion efficiency of 3.9% when as-prepared 10-μm-thick ZnO films were sensitized by N719 dye with an immersion time of 2 h.<sup>[88]</sup> Further improvement to 4.27% in the conversion efficiency was reported recently by Hosono et al. when the dye of N719 was replaced with a metal-free organic dye named D149 and the immersion time was reduced to 1 h.<sup>[92]</sup> The enhancement in solar-cell performance was attributed to the use of D149 dye and a nanoporous structure that contained perpendicular pores. This allowed for a rapid adsorption of the dye with a shorter immersion time and thus prevented the formation of a Zn<sup>2+</sup>/dye complex. This complex is believed to be inactive and may hinder electron injection from the dye molecules to the semiconductor.<sup>[73]</sup> In another study, a high photovoltaic efficiency of up to 4.1% was also obtained for nanoporous ZnO films produced by the CBD.<sup>[90]</sup> However, the excellence of the solar-cell performance was ascribed to the remarkably improved stability of as-fabricated ZnO films in acidic dye. According to this report, a 20-μm-thick ZnO film prepared via CBD was used for the DSC and the film was sensitized with N719. The results showed that, even for a prolonged dye-loading time (6 h), only a monolayer of dye molecules adsorbed on the ZnO surface and no Zn<sup>2+</sup>/dye complex was formed. This scenario is very different from the case of ZnO films sensitized with ruthenium-based dye reported elsewhere and has resulted in a relatively high overall conversion efficiency. It was also demonstrated that, for this cell, the dye-loading amount was estimated to be about 1.4 × 10<sup>-7</sup> mol cm<sup>-2</sup>. This was comparable to the 1.3 × 10<sup>-7</sup> mol cm<sup>-2</sup> obtained for a 10-μm-thick nanocrystalline TiO<sub>2</sub> photoanode (η = 10%) sensitized with N3 dye. In this study, although approximately equal dye

loading is obtained for ZnO films with doubled thickness ( $\approx 20 \mu\text{m}$ ) in comparison to  $\approx 10 \mu\text{m}$  of  $\text{TiO}_2$ , the results are very exciting in view of the unusual stability of as-prepared ZnO in ruthenium-based dyes.

### 2.3. Other Nanostructured ZnO Films

ZnO nanostructures with other morphologies, such as nanosheets, nanobelts, and nanotetrapods, have also been studied for DSC applications on account of the fact that they also have a large specific surface area. However, for these nanostructures, the specific surface area is not the only factor that determines the photovoltaic efficiency of the DSC. Solar-cell performance is also believed to be significantly affected by the geometrical structure of the photoelectrode films, which provides particular properties in terms of the electron transport and/or light propagation.

#### 2.3.1. Nanosheets

ZnO nanosheets are quasi-two-dimensional structures that can be fabricated by a rehydrothermal growth process of previously hydrothermally grown ZnO nanoparticles.<sup>[93]</sup> A film with dispersed ZnO nanosheets (Fig. 4a) used in a DSC has been shown to possess a relatively low conversion efficiency, 1.55%, possibly due to an insufficient internal surface area. It seems that ZnO nanosheet-spheres (Fig. 4b) prepared by hydrothermal treatment using oxalic acid as the capping agent may have a significant enhancement in internal surface area, resulting in a conversion efficiency of up to 2.61%.<sup>[94]</sup> As for nanosheet-spheres, the performance of the solar cell is also believed to benefit from a high degree of crystallinity and, therefore, low resistance with regards to electron transport.

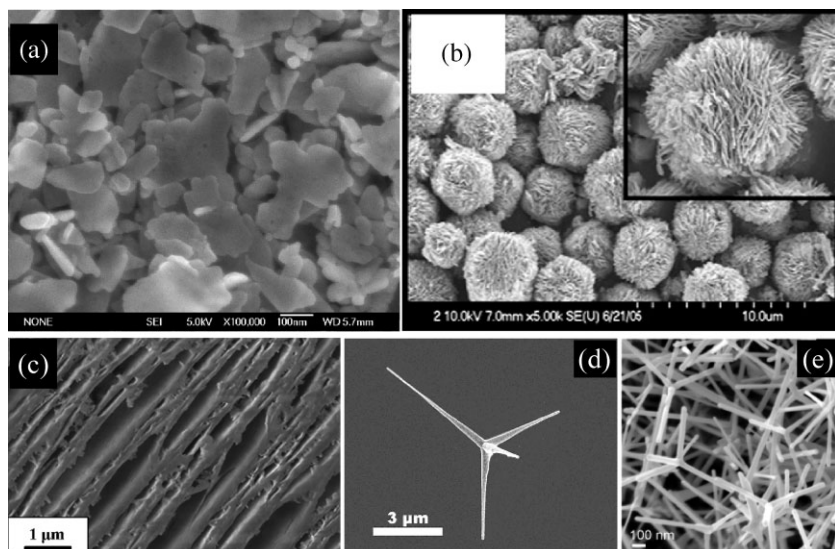


**Figure 4.** SEM images of nanostructured ZnO films: a) Dispersed nanosheets. Reproduced with permission from [93]. Copyright 2007, Elsevier. b) Nanosheet-assembled spheres. Reproduced with permission from [94]. Copyright 2008, Elsevier. c) Nanobelt array. Reproduced with permission from [95]. Copyright 2007, Elsevier. d) A ZnO tetrapod formed in a three-dimensional structure with four arms extending from a common core. Reproduced with permission from [96]. Copyright 2008, American Institute of Physics. e) Networked film with interconnected ZnO tetrapods. Reproduced with permission from [97]. Copyright 2009, Elsevier.

#### 2.3.2. Nanobelts

ZnO films with nanobelt arrays prepared through an electro-deposition method were also studied for DSC applications.<sup>[95]</sup> In fabricating these nanobelts, polyoxyethylene cetyether was added in the electrolyte as a surfactant. The ZnO nanobelt array obtained shows a highly porous stripe structure (Fig. 4c) with a nanobelt thickness of 5 nm, a typical surface area of  $70 \text{ m}^2 \text{ g}^{-1}$ , and a photovoltaic efficiency as high as 2.6%.

#### 2.3.3. Tetrapods

A ZnO tetrapod possesses a three-dimensional structure consisting of four arms extending from a common core (Fig. 4d).<sup>[96,97]</sup> The length of the arms can be adjusted within the range of 1–20  $\mu\text{m}$ , while the diameter can be tuned from 100 nm to 2  $\mu\text{m}$  by changing the substrate temperature and oxygen partial pressure during vapor deposition.<sup>[98]</sup> Multiple-layer deposition can result in tetrapods connected to each other so as to form a porous network with a large specific surface area (Fig. 4e). The films with ZnO tetrapods used in DSCs have achieved overall conversion efficiencies of 1.20–3.27%.<sup>[96,97]</sup> It was reported that the internal surface area of tetrapod films could be further increased by incorporating ZnO nanoparticles with these films, leading to significant improvement in the solar-cell performance.<sup>[96]</sup>

## 3. Nanostructures with Direct Pathways for Electron Transport

Electron transport in DSCs based on nanoparticulate films has been proposed to occur either by a series of hopping events between trap states on neighboring particles<sup>[99]</sup> or by diffusive transport within extended states slowed down by trapping/detrapping events.<sup>[21,30]</sup> An electron is estimated to cross  $10^3$ – $10^6$  particles when traveling in the photoelectrode film.<sup>[99]</sup> While an 11% efficiency has been achieved on dye-sensitized  $\text{TiO}_2$  nanocrystalline films, the nanoparticulate oxides do possess deficiencies. Electron transport becomes more difficult with an increase in photocurrent due to the also-increased recombination between the electrons and the oxidized dye or redox mediator in the electrolyte.<sup>[100]</sup> Recombination, intrinsically, arises from the absence of a depletion layer at the  $\text{TiO}_2$  nanoparticle–electrolyte interface. In DSCs with a film in the form of nanoparticles, the recombination has been found to be a crucial factor that causes energy loss and limits the further increase of conversion efficiency.<sup>[101]</sup>

In the past few years, a variety of one-dimensional nanostructures based on different oxides have been developed so as to reduce the recombination rate in DSCs.<sup>[102]</sup> These one-dimensional nanostructures are usually single crystal or quasi single crystal and can,

therefore, serve to increase the electron diffusion length by providing a direct pathway for electron transport from the point of electron injection to the substrate of the collection electrode. In other words, the transport of electrons occurs in the interior of a continuous crystal and, consequently, the electrons would not suffer any grain-boundary scattering. This is different from the case of nanoparticulate films in a DSC configuration, where electrons, during their traversal, take a random walk among the nanoparticles and undergo numerous collisions at the grain boundary or the semiconductor/electrolyte interface. Among all the oxides with one-dimensional nanostructures, ZnO has been the most reported due to the ease of controllable anisotropic growth and, especially, the development of physical or chemical techniques that allow for a flexible tailoring of ZnO morphology (for example, shape, diameter, length, density, etc.). Typical one-dimensional ZnO nanostructures used for DSCs involve types of nanowires/nanorods, nanotubes, nanotips, and other derivatives, synthesized through vapor–liquid–solid processes,<sup>[55]</sup> metal–organic chemical vapor deposition (MOCVD),<sup>[103,104]</sup> thermal evaporation,<sup>[104,105]</sup> chemical-solution synthesis at low temperature,<sup>[106]</sup> electrodeposition,<sup>[107,108]</sup> and chemical-spray pyrolysis.<sup>[109]</sup> In general, the vapor-phase or physical-deposition methods possess an inherent advantage in forming both thin and long one-dimensional nanostructures with a high degree of crystal quality while affording the ability to precisely control the growth rate. Chemical-solution-based methods possess the capability for large-scale mass production at low temperatures and, therefore, a flexible substrate can be used.

### 3.1. ZnO Nanowires

ZnO nanowire arrays were first used in DSCs by Law et al. in 2005 with the intention of replacing the traditional nanoparticle film with a consideration of increasing the electron diffusion length.<sup>[110,111]</sup> A schematic of the construction of a nanowire DSC is shown in Figure 5a. Arrays of ZnO nanowires were synthesized in an aqueous solution using a seeded-growth process. This method employed fluorine-doped tin oxide (FTO) substrates that were thoroughly cleaned by acetone/ethanol sonication. A thin film of ZnO quantum dots (dot diameter = 3–4 nm, film thickness = 10–15 nm) was deposited on the substrates via dip coating in a concentrated ethanol solution.

Nanowires were grown by immersing the seeded substrates in aqueous solutions containing 25 mM zinc nitrate hydrate, 25 mM hexamethylenetetramine, and 5–7 mM polyethylenimine (PEI) at 92 °C for 2.5 h. After this period, the substrates were repeatedly introduced to fresh solution baths in order to obtain continued growth until the desired film thickness was reached. The use of PEI, a cationic polyelectrolyte, is particularly important in this fabrication, as it serves to enhance the anisotropic growth of nanowires. As a result, nanowires synthesized by this method possessed aspect ratios in excess of 125 and densities up to 35 billion wires per square centimeter. The longest arrays reached 20–25 μm with a nanowire diameter that varied from 130 to 200 nm. These arrays featured a surface area up to one-fifth as large as a nanoparticle film. Figure 5b shows a typical SEM cross-section image of an array of ZnO nanowires. It was found that the resistivity values of individual nanowires ranged from 0.3 to 2.0 Ω cm, with an electron concentration of  $1\text{--}5 \times 10^{18} \text{ cm}^{-3}$  and a mobility of  $1\text{--}5 \text{ cm}^2 \text{ V}^{-1} \text{ s}^{-1}$ . Consequently, the electron diffusivity could be calculated as  $0.05\text{--}0.5 \text{ cm}^2 \text{ s}^{-1}$  for a single nanowire. This value is several hundred times larger than the highest reported electron diffusion coefficients for nanoparticle films in a DSC configuration under operating conditions, that is,  $\approx 10^{-7}\text{--}10^{-4} \text{ cm}^2 \text{ s}^{-1}$  for TiO<sub>2</sub> and  $\approx 10^{-5}\text{--}10^{-3} \text{ cm}^2 \text{ s}^{-1}$  for ZnO. This, to some extent, demonstrates the very good electrical conductivity of ZnO nanowires. (It must be noted, however, that the electron diffusivity and the electron diffusion coefficient reflect different charge transport processes in individual nanowires and nanoparticle films, respectively. Moreover, these two parameters are usually obtained through different methods, that is, by employing the Einstein equation with the measured Hall mobility to calculate the electron diffusivity for individual nanowires and using, for example, intensity-modulated photocurrent experiments to measure the collection time of electron diffusion and then calculate the electron diffusion coefficient for nanoparticle films.<sup>[47,112]</sup>) At a full sun intensity of  $100 \pm 3 \text{ mW cm}^{-2}$ , the highest-surface-area devices with ZnO nanowire arrays were characterized by short-circuit current densities of 5.3–5.85 mA cm<sup>-2</sup>, open-circuit voltages of 610–710 mV, fill factors of 0.36–0.38, and overall conversion efficiencies of 1.2–1.5%.

The superiority of ZnO nanowires as a direct pathway for electron transport is illustrated by Figure 5c, in which the short-circuit current densities as a function of the internal

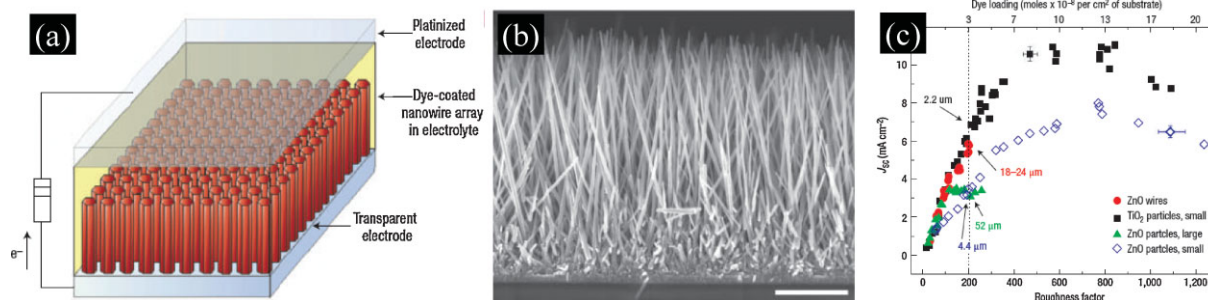


**Figure 5.** ZnO-nanowire dye-sensitized solar cells. Reproduced with permission from [110]. Copyright 2005, Nature Publishing Group. a) Schematic diagram of the cell with a photoelectrode comprised of the ZnO-nanowire array. b) Cross-sectional SEM image of the ZnO-nanowire array. c) Comparative performance of nanowire and nanoparticle cells.

roughness factor (defined as the ratio of actual surface area to the projected surface area) are compared for cells with ZnO nanowires, TiO<sub>2</sub> nanoparticles, and ZnO nanoparticles. The plot shows that a rapid saturation and a subsequent decline in the short-circuit current density can be observed on the cells built with either 12-nm TiO<sub>2</sub> nanoparticles or 30-nm and 200-nm ZnO nanoparticles. This confirms that the transport efficiency of nanoparticle films falls off above a certain film thickness due to critical recombination. However, the nanowire films show a nearly linear increase in the short-circuit density that maps almost directly onto the TiO<sub>2</sub> data even though the films are as thick as  $\approx 25 \mu\text{m}$ , indicating a highly efficient transport of electrons in nanowires with decreased recombination rate. In addition, the nanowire cells generate considerably higher current densities than the ZnO nanoparticle cells over the accessible range of roughness factors (approximately 55–75% higher at a roughness of 200, as shown in Fig. 5c). This is also a confirmation that the nanowires offer better electron transport when compared to nanoparticles. The mechanism has been attributed to both the high crystallinity of nanowires and an internal electric field within the nanowires that can assist carrier collection by separating injected electrons from the surrounding electrolyte and sweeping them towards the collection electrode. The establishment of an internal electric field within the nanowires is due to the existence of charge diffusion at the semiconductor–electrolyte interface and the formation of a space-charge layer in the nanowires around the inner surface. In oxide semiconductors, the Debye screening length, which is defined as the distance over which significant charge separation can occur, has been estimated to be roughly one-third of the thickness of the space-charge layer.<sup>[110]</sup> As for ZnO with a carrier concentration of  $10^{18} \text{cm}^{-3}$ , the Debye screening length is about 4 nm. It is important that the dimension of the as-discussed ZnO nanowires is much larger than the Debye screening length so that an internal electric field can be established. Owing to the upward band bending in the nanowires around the inner surface, the internal electric field is thought to be able to (1) corral the injected electrons so as to reduce the recombination rate, and (2) accelerate the diffusion of injected electrons towards the interior of the nanowires. Moreover, the axial field may serve to sweep the electrons to the collection electrode. Similar investigations can be found elsewhere in literature regarding the application of ZnO nanowires in DSCs even with the attainment of higher conversion efficiencies.<sup>[113–118]</sup> However, it seems that the results are quite dependent on the experimental conditions, specifically on the synthesis method, substrate treatment, growth parameters, geometrical structure of the nanowires and array (pattern, diameter, length, density, etc.), and the measuring method (sensitization process, electrolyte composition, light-source intensity, and active area of photoelectrode film, etc.).

Besides the one-dimensional structure of nanowires/nanorods, the feature of nanowire/nanorod arrays with vertically aligned growth on the FTO substrate is also addressed as one of important aspects that provide the direct pathway for electron transport in DSCs. This has been demonstrated convincingly in previous research. For example, one study found that a ZnO nanorod array led to a ten-fold increase in the photovoltaic efficiency when compared to a randomly oriented nanorod film.<sup>[119]</sup> However, the insufficient surface area of nanowire/

nanorod arrays seems to be the primary factor that limits the amount of dye adsorption as well as the conversion efficiency of the cells. Many attempts have been made to solve this problem. One such approach is to reduce the diameter size of the nanowires/nanorods, thus increasing the density of the array.<sup>[113,116,117]</sup> Gao et al. reported a simple method that employed ammonium hydroxide to change the supersaturation degree of Zn<sup>2+</sup> precursors during the process of solution-based growth of a ZnO nanowire array. This served to regulate the length-to-diameter aspect ratio of the individual nanowires. The resulting nanowires possessed an aspect ratio of about 100–200 with a length of 14  $\mu\text{m}$  and a diameter of 120–150 nm. This led to an overall DSC conversion efficiency of 1.7%, which is almost three times that obtained for ZnO nanorod arrays with relatively low aspect ratios (about 500 nm in diameter and 10  $\mu\text{m}$  in length).<sup>[120]</sup> By blending the nanowires with nanoparticles, ZnO nanowire–nanoparticle-composite films have been also proved to be effective in optimizing the surface area. Ku et al. reported a significant promotion in the overall DSC conversion efficiency from 0.84% to 2.2% when ZnO nanoparticles with diameters of 5–30 nm were added to ZnO nanowires.<sup>[121]</sup> As for the fabrication of nanowire–nanoparticle-composite films, a pretreatment performed by immersing the ZnO nanoparticle powder in a methanol solution containing 2% titanium isopropoxide and 0.02 M acetic acid has proved to be favorable for the attachment of nanoparticles onto nanowire surfaces.<sup>[122]</sup>

### 3.2. ZnO Nanotubes

Nanotubes differ from nanowires in that they typically have a hollow cavity structure. An array of nanotubes possesses high porosity and may offer a larger surface area than that of nanowires. The synthesis of ZnO nanotube arrays can be achieved by using a modified method for the aqueous growth of ZnO nanowires at low temperatures.<sup>[56,123]</sup> An overall conversion efficiency of 2.3% has been reported for DSCs with ZnO nanotube arrays possessing a nanotube diameter of 500 nm and a density of  $5.4 \times 10^6$  per square centimeter.<sup>[124]</sup> ZnO nanotube arrays can be also prepared by coating anodic aluminum oxide (AAO) membranes via atomic layer deposition (ALD). However, it yields a relatively low conversion efficiency of 1.6%, primarily due to the modest roughness factor of commercial membranes.<sup>[125]</sup>

### 3.3. ZnO Nanotips

By using MOCVD processing methods, ZnO nanotip arrays with different lengths can be synthesized. The DSC performance of these nanotips has been investigated in previous studies.<sup>[126,127]</sup> The results confirmed that the energy-conversion efficiency of the cells increased with the length of the ZnO nanotips due to the increase in surface area of the photoelectrode film. An overall conversion efficiency of 0.55% was obtained for 3.2- $\mu\text{m}$ -long ZnO nanotips. It has been reported that ZnO nanotips present a maximum overall conversion efficiency at higher light intensities than in the case of TiO<sub>2</sub> nanoparticles. This implies a nontrap-limited electron transport in the respect that the nanotips provide a faster conduction pathway for electron transport. This

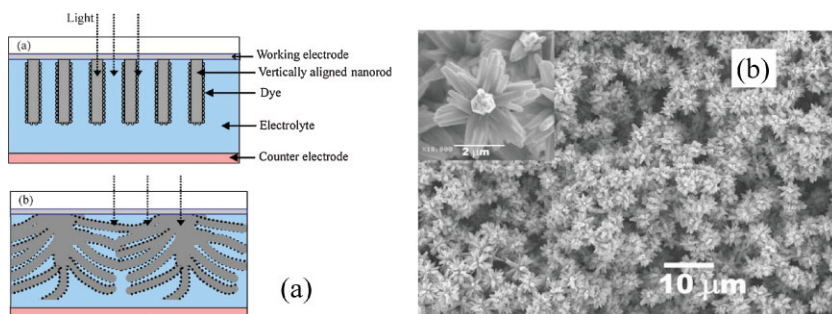


**Figure 6.** Flower-like ZnO nanostructures. a) A schematic to indicate the difference in light harvest for films with nanowires and nanoflowers. b) SEM images of a ZnO-nanoflower film. Reproduced with permission from [128]. Copyright 2007, American Institute of Physics.

feature allows for the use of ZnO nanotips in the fabrication of more stable and efficient DSCs under high illumination. It has also been demonstrated that the overall conversion efficiency could be increased to 0.77% by combining the ZnO nanotips with a Ga-doped ZnO film as a transparent conducting layer.<sup>[127]</sup>

### 3.4. ZnO “Nanoflowers”

The use of ZnO films with “nanoflowers” consisting of upstanding nanowires and outstretched branches have been also reported for application in DSCs. This is based on the consideration that the nanowires alone may not capture the photons completely due to the existence of intervals inherent in the morphology. Nanoflower structures, however, have nanoscale branches that stretch to fill these intervals and, therefore, provide both a larger surface area and a direct pathway for electron transport along the channels from the branched “petals” to the nanowire backbone (Fig. 6). Nanoflower films can be grown by a hydrothermal method at low temperatures, typically by employing a 5 mM zinc chloride aqueous solution with a small amount of ammonia.<sup>[128]</sup> These as-synthesized nanoflowers, as shown in Figure 6b, have dimensions of about 200 nm in diameter. The solar-cell performance of ZnO nanoflower films was characterized by an overall conversion efficiency of 1.9%, a current density of  $5.5 \text{ mA cm}^{-2}$ , and a fill factor of 0.53. These values are higher than the 1.0%,  $4.5 \text{ mA cm}^{-2}$ , and 0.36 for films of nanorod arrays with comparable diameters and array densities that were also fabricated by the hydrothermal method.<sup>[129]</sup>

### 3.5. Dendritic ZnO Nanowires

Dendritic ZnO nanowires, which possess a fractal structure more complicated than that of nanoflowers, are formed by a nanowire backbone with outstretched branches, on which the growth of smaller-sized nanowire backbones and branches is reduplicated. Baxter et al. described a MOCVD fabrication for dendritic ZnO nanowires by using a route of so-called multiple-generation growth.<sup>[103]</sup> They first

grew 100-nm-diameter ZnO nanowires with 20-nm secondary nanowire branches that nucleated and grew from the primary nanowire backbone. It was indicated that each of the nanowires was crystalline with grain boundaries separating secondary nanowires from the primary nanowire. The substrate with both primary nanowires and secondary nanowire branches was then used to continue the nanowire growth, called “secondary generation” growth. During the growth of a second generation of nanowires, the outstretched nanowire branches act as new nucleation sites for nanowire growth. The growth can also be continued for third and fourth generations for

the attainment of a dendrite-like branched ZnO nanostructure (Fig. 7). DSC characterization showed that the short-circuit density increased with increasing growth generation due to the larger surface area, which in turn led to increased adsorption of dye molecules. A total improvement of over 250 times in current density and over 400 times in efficiency has been observed when the film morphology was changed from smooth nanowires to branched second-generation nanowires (Fig. 7b). The efficiencies obtained using fourth-generation dendritic nanowire films with a branched nanostructure and a  $10\text{-}\mu\text{m}$  thickness displayed an overall conversion efficiency of 0.5%, a more than 600-fold improvement over smooth nanowires. By integrating ZnO nanoparticles within the film of dendritic nanowires, the specific surface area was increased, leading to an improved conversion efficiency of 1.1% for these cells.

The dendritic ZnO nanowires are intentionally developed to increase the specific surface area of the photoelectrode film by multiple-generation growth of ZnO nanowires. However, the photovoltaic efficiency, 0.5%, obtained for dendritic ZnO nanowires is lower than the 1.5% value for ZnO nanowire arrays achieved by Law et al. This is possibly due to the lower nanowire density and the insufficient nanowire length (or aspect ratio) of dendritic ZnO nanowires. Another possible cause is the difference in the crystallinity of nanowires produced by different fabrication methods, that is, MOCVD for dendritic ZnO nanowires and seed-assisted solution-based epitaxy growth for ZnO nanowire arrays.

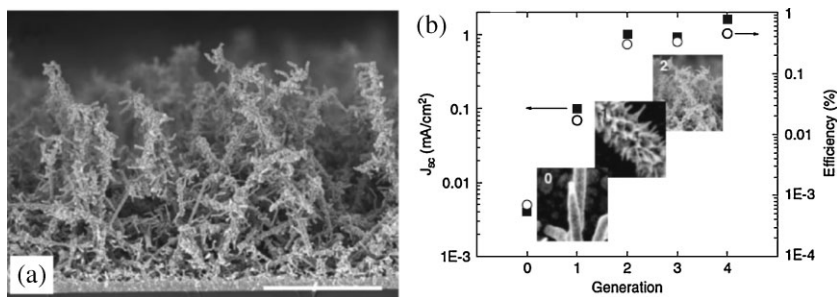


**Figure 7.** Dendritic ZnO nanowires for DSC application. a) Cross-sectional SEM image of a film with dendritic ZnO nanowires (after two generations of growth). b) Semi-log plot of short-circuit current (filled squares) and efficiency (open circles) versus nanowire growth generation, with insets showing images of nanowire morphology for generations 0–2. Reproduced with permission from [103]. Copyright 2005, Elsevier.

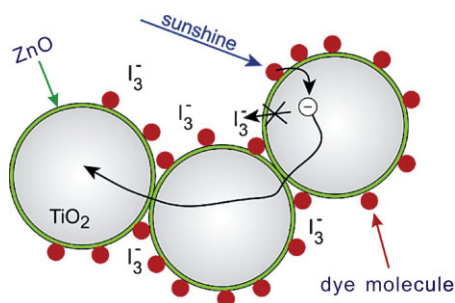


**Figure 8.** Schematic of a typical  $\text{TiO}_2$ -ZnO core-shell structure used in DSCs. The ZnO shell provides an energy barrier at the interface between the  $\text{TiO}_2$  and the dye or electrolyte to reduce the recombination of electrons with oxidized dye molecules or those accepting species in the electrolyte. Reproduced with permission from [130]. Copyright 2004, American Chemical Society.

#### 4. Core-Shell Structures with ZnO Shell for Reduced Recombination Rate

Core-shell structures are a configuration designed for electrode films in DSCs to reduce the recombination rate at the electrode/electrolyte interface. A core-shell nanostructured electrode usually consists of a nanoporous  $\text{TiO}_2$  matrix that is covered with a shell of another metal oxide or salt (Fig. 8).<sup>[130]</sup> The conduction-band potential of the shell should be more negative than that of the core semiconductor ( $\text{TiO}_2$ ). This establishes an energy barrier which hinders the reaction of electrons in the core with the oxidized dye or redox mediator in the electrolyte.<sup>[131]</sup> Several shell materials such as ZnO,  $\text{Al}_2\text{O}_3$ ,  $\text{SiO}_2$ ,  $\text{Nb}_2\text{O}_5$ ,  $\text{WO}_3$ , MgO,  $\text{SrTiO}_3$ , and  $\text{CaCO}_3$  have been reported to form an energy barrier (or a surface dipole layer) on  $\text{TiO}_2$ , enhancing the solar-cell performance by providing a 35% increase in the overall conversion efficiency.<sup>[132–143]</sup> Among all those materials studied, ZnO has been attracting the most attention in view of its low electron affinity, high isoelectric point, and more negative conduction-band edge when compared to  $\text{TiO}_2$ .

##### 4.1. Fabrication of Core-Shell Structures and Influence of Shell Thickness

There have been several reports on the fabrication of ZnO shells for the  $\text{TiO}_2$  surface. In general, the fabrication approach of core-shell structures can be classified into two cases. One involves the initial synthesis of core-shell structured  $\text{TiO}_2$ -ZnO nanoparticles and then application onto a conducting substrate so as to obtain a film.<sup>[135,144]</sup> The consequence of this fabrication method is the formation of an energy barrier not only at the electrode-electrolyte interface but also between the individual  $\text{TiO}_2$  particles. Thus, at least conceptually, resistance to the transport of photoinjected electrons through the  $\text{TiO}_2$  network should increase. In a second approach, a nanoporous  $\text{TiO}_2$  electrode film is fabricated. This film then serves as a matrix for coating of a thin ZnO shell layer.<sup>[145,146]</sup> As a result, the core particles are connected directly to each other, allowing for electron transport through the  $\text{TiO}_2$  network.

Wang et al. reported a hydrothermal method for the formation of  $\text{TiO}_2$ -ZnO nanoparticles with a core-shell structure.<sup>[135]</sup> The researchers mixed 0.5 mol %  $\text{ZnCl}_2$  with 2M  $\text{TiCl}_4$  aqueous solution and adjusted the pH value to 5 with KOH. After hydrothermal growth at 170 °C and annealing of the precipitates at 450 °C, 0.46 mol % ZnO was found in the  $\text{TiO}_2$ -Zn product. Transmission electron microscopy (TEM) images revealed the  $\text{TiO}_2$  nanoparticles to be about 10 nm in diameter and that the covering layer of ZnO had no influence on the growth of  $\text{TiO}_2$  nanoparticles. X-ray diffraction (XRD) analysis indicated that the ZnO-covered  $\text{TiO}_2$  was still in the pure anatase phase and no separated ZnO phase (or other phase) was detected. Therefore, the possibility of  $\text{Zn}^{2+}$  substituting the lattice position of  $\text{Ti}^{4+}$  was excluded and it was inferred that the  $\text{Ti}^{4+}$  ions were first precipitated, followed by the precipitation of  $\text{Zn}^{2+}$  on the  $\text{TiO}_2$  surface. The  $\text{Zn}^{2+}$  forms ZnO after annealing. Based on a similar mechanism, Kim et al. also reported a simple route to obtain a ZnO shell on  $\text{TiO}_2$  nanoparticles by directly soaking the  $\text{TiO}_2$  powder (Degussa, P25) in a 10 mM solution of  $\text{ZnCl}_2$  in absolute ethanol. This suspension solution was then sprayed into liquid  $\text{N}_2$ . A powder sample was finally obtained after a freeze-drying process, followed by sintering at 500 °C.<sup>[144]</sup> The thickness of the ZnO layer synthesized by this method was measured to be  $\approx 0.50$  nm, which was thin enough for electron tunneling in the process of particle-to-particle transport.

By first preparing the  $\text{TiO}_2$  nanocrystalline film and then depositing the ZnO shell using a layer-by-layer technique, Han et al. made a series of systematic studies on the construction of ZnO shells with varying thicknesses.<sup>[145,147]</sup> The influence of this parameter was evaluated with regards to DSC performance. It was found that, for  $\text{TiO}_2$  photoelectrodes coated with a 30-nm-thick ZnO layer, the overall conversion efficiency reached 4.51%, while it was 3.31% for bare  $\text{TiO}_2$  without modification. The thickness of the ZnO shell could significantly affect the short-circuit density, which decreased when the shell thickness turned out to be larger than 30 nm, partially because of the small effective mass of electrons ( $\approx 0.3 m_e$ ) in ZnO.<sup>[148,149]</sup> A radio frequency (RF)-magnetron sputtering method was also reported for the deposition of a ZnO coating layer on the  $\text{TiO}_2$  nanocrystalline films.<sup>[150]</sup> It was demonstrated that the conversion efficiency of  $\text{TiO}_2$  DSCs was improved from 4.76% to 6.55% due to the ZnO modification.

##### 4.2. The Role of the ZnO Shell

As for core-shell structures in DSC applications, the role of the ZnO shell has most often been demonstrated to provide an energy barrier at the interface between the  $\text{TiO}_2$  and the dye or electrolyte, so as to reduce the recombination of electrons with oxidized dye molecules or those accepting species in the electrolyte. Fig. 9 presents an energy-level diagram that schematically indicates the function of the ZnO shell in a  $\text{TiO}_2$ -ZnO core-shell structure.<sup>[147]</sup> That is, the bottom of conduction band ( $-4.0$  eV) and the top of valence band ( $-6.8$  eV) of ZnO are lower than the lowest unoccupied molecular orbital (LUMO,  $-3.8$  eV) and the highest occupied molecular orbital (HOMO,  $-5.4$  eV) energy levels of the dye, and are also higher than those of  $-4.2$  eV and  $-7.4$  eV for  $\text{TiO}_2$ , respectively. Those photogenerated electrons in the dye molecules with high kinetic

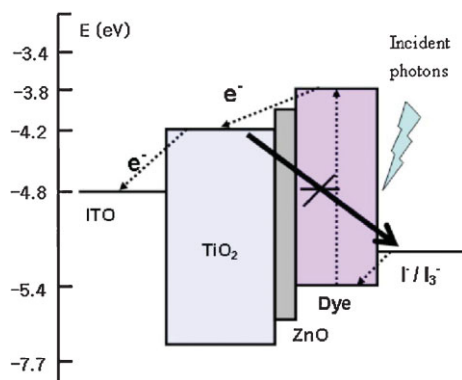


**Figure 9.** Schematic diagram of the energy levels of a core-shell-structured ( $\text{TiO}_2$ - $\text{ZnO}$ ) photoelectrode in DSCs. Reproduced with permission from [147]. Copyright 2006, American Institute of Physics.

energy can readily tunnel through the ZnO shell and inject into the  $\text{TiO}_2$ . However, the transport of electrons in the reverse direction may be blocked due to the presence of an energy barrier provided by the ZnO shell, thereby reducing the recombination rate of photogenerated electrons.

Although the energy-barrier model can sufficiently explain the enhanced DSC performance by ZnO-coated  $\text{TiO}_2$ , Zaban et al.<sup>[131,137]</sup> and Bandara et al.<sup>[151]</sup> believe that this enhancement results from the conduction-band-shift mechanism, rather than the formation of an energy barrier at the surface. The shift of the  $\text{TiO}_2$  conduction band is attributed to the existence of a dipole layer at the electrode-electrolyte interface due to the differences between the shell and core materials with respect to the higher isoelectric point and lower electron affinity of ZnO compared to  $\text{TiO}_2$ . Thus, the  $\text{TiO}_2$  conduction band is moved towards a relatively negative direction, resulting in a higher open-circuit voltage for the DSCs. Some arguments insist that the enhancement of the ZnO shell with regards to the DSC performance is a result of the prolonged lifetime of photogenerated electrons in ZnO over that in  $\text{TiO}_2$ . Hagfeldt et al. studied charge-transport properties in a nanostructured ZnO thin-film electrode-electrolyte system with time-resolved laser-flash-induced photocurrents and compared with results on  $\text{TiO}_2$ . They observed that the electrons existed longer in ZnO than in  $\text{TiO}_2$ , and thus the electron losses to acceptors in the electrolyte were less for ZnO than for  $\text{TiO}_2$ .<sup>[152,153]</sup> In addition, the ZnO shell has been proposed to increase the free-electron concentration in the conduction band with respect to pure  $\text{TiO}_2$  based on an experimental observation that the electrode of  $\text{TiO}_2$  with a ZnO coating presents an optical absorbance larger than that for  $\text{TiO}_2$  alone.<sup>[135]</sup> It is thought that the optical absorbance is proportional to the concentration of free electrons in the conduction band of the semiconductor while the electrode is characterized by using a variable-potential spectroscopy technique developed by Rothenberger et al.<sup>[154]</sup>

However, opinions can also be found in literature that deny the improvement in efficiency of  $\text{TiO}_2$ -based DSCs by forming outer-shell structures of insulator or semiconductor materials.<sup>[130,155]</sup> These viewpoints originate from experimental phenomena showing that ZnO modification of nanocrystalline  $\text{TiO}_2$  may indeed increase the open-circuit voltage, but may also

simultaneously cause a decrease in the short-circuit current density, ultimately resulting in a reduced conversion efficiency. This has been explained by either poor dye adsorption to zinc sites on the  $\text{TiO}_2$  surface or a low electron-injection efficiency due to the buildup of a thin insulating ZnO surface layer. As such, the role of the ZnO shell on the  $\text{TiO}_2$  surface is still under discussion. The difference in the observed effects of the ZnO shell is perhaps due to the dye adsorption and the electron injection process that are both sensitive to the surface or interface of semiconductors. Also, the status of the ZnO shell is quite dependent on the fabrication method as well as other experimental variables.

## 5. Light Scattering Enhancement Effect

In DSCs, the dynamic competition between the generation and recombination of photoexcited carriers has been found to be a bottleneck restricting the development of higher conversion efficiencies. That is, the film thickness was expected to be larger than the light-absorption length so as to capture more photons. Furthermore, the film thickness was constrained to be smaller than the electron-diffusion length so as to avoid or reduce recombination.<sup>[31,32]</sup> The approaches outlined above serve mostly to overcome the recombination by either using one-dimensional nanostructures that provide a direct pathway for electron transport or using core-shell structures with an oxide coating on  $\text{TiO}_2$  to minimize the recombination rate. Besides those approaches, a series of methods that address the generation of photoexcited carriers by combining nanostructured films with optical effects (light scattering or optical confinement)<sup>[156]</sup> have also been demonstrated to be effective in enhancing the light-harvesting capability of the photoelectrode film so as to improve DSC performance.

Usami,<sup>[157]</sup> Ferber and Luther,<sup>[158]</sup> and Rothenberger et al.<sup>[159]</sup> theoretically demonstrated that the optical absorption of dye-sensitized nanocrystalline  $\text{TiO}_2$  films could be promoted by additionally admixing large-sized  $\text{TiO}_2$  particles as the light-scattering centers. The light-scattering efficiency has been shown to correlate with both the size of the scattering centers and the wavelength of the incident light.<sup>[160]</sup> The scattering reaches a maximum when the size of the scattering centers is about  $k\lambda$ , where  $k$  is a constant and  $\lambda$  is the wavelength. Experimentally, it has been verified that the performance of DSCs can be significantly improved when the  $\text{TiO}_2$  nanocrystalline films are combined with large-sized  $\text{SiO}_2$ ,  $\text{Al}_2\text{O}_3$ , or  $\text{TiO}_2$  particles.<sup>[161-165]</sup> By coupling a photonic-crystal layer to conventional  $\text{TiO}_2$  nanocrystalline films for light scattering, Nishimura et al.<sup>[166]</sup> and Halaoui et al.<sup>[167]</sup> also succeeded in enhancing the light-harvesting capability of the photoelectrode. However, the introduction of large-sized particles into nanocrystalline films has the unavoidable effect of lowering the internal surface area of the photoelectrode film. This serves to counteract the enhancement effect of light scattering on the optical absorption, whereas the incorporation of a photonic-crystal layer may lead to an undesirable increase in the electron transport length and, consequently, increase the recombination rate of photogenerated carriers. A recently reported hierarchically structured film with ZnO aggregates, which provides the photoelectrode with both a large surface area and efficient light-scattering centers, can, to

some extent, resolve such an inconsistency. When this type of nanostructured film was used for DSCs, a very impressive enhancement in the overall conversion efficiency was observed.<sup>[168–170]</sup>

### 5.1. ZnO Aggregates

Hierarchically structured ZnO films consist of submicrometer-sized ZnO aggregates. The synthesis of ZnO aggregates can be achieved by hydrolysis of zinc salt in a polyol medium at 160 °C.<sup>[168]</sup> By adjusting the heating rate during synthesis and using a stock solution containing ZnO nanoparticles of 5 nm in diameter, ZnO aggregates with either a monodisperse or polydisperse size distribution can be prepared.<sup>[169,170]</sup> Fig. 10 shows the morphology of a hierarchically structured ZnO film and the structure of the aggregates. It can be seen that the film is

well packed by ZnO aggregates with a highly disordered stacking, while the spherical aggregates are formed by numerous interconnected nanocrystallites that have sizes ranging from several tens to several hundreds of nanometers (Fig. 10b and c). The structural features of the aggregates are their possession of a porosity and geometrical size comparable with the wavelengths of visible light. Four kinds of ZnO films, differing in the degree of aggregation, were prepared for a comparison of their DSC performance. Sample 1 is comprised of well-packed polydisperse ZnO aggregates, sample 2 consists of aggregates with slight distortion of the spherical shape, sample 3 includes parts of aggregates and nanocrystallites, and sample 4 is constructed with no aggregates but dispersed nanocrystallites alone. It has been demonstrated that all these samples present approximately the same crystallite size of about 15 nm and similar specific surface area of  $\approx 80 \text{ m}^2 \text{ g}^{-1}$ . However, their photovoltaic behaviors exhibit a significant difference in the short-circuit current density,

resulting in a difference of overall conversion efficiency. Typically, a maximum short-circuit current density of  $19 \text{ mA cm}^{-2}$  and conversion efficiency of 5.4% are observed for sample 1, while minimum values of  $10 \text{ mA cm}^{-2}$  and 2.4% respectively are observed for sample 4. Intermediate current densities and efficiencies are found for samples 2 and 3 (Fig. 10d). An obvious trend is that the overall conversion efficiency decreases as the degree of the spherical aggregation is gradually destroyed. In other words, the aggregation of ZnO nanocrystallites is favorable for achieving a DSC with high performance.

Figure 10e shows the optical-absorption spectra of the four kinds of ZnO films previously discussed after being sensitized with N3 dye. All the ZnO samples exhibit an intrinsic absorption with similar absorption intensity below 390 nm, caused by the ZnO semiconductor with electron transfer from the valence band to the conduction band. However, absorption at wavelengths above 400 nm varies significantly, revealing the highest intensity for sample 1, a lower intensity for samples 2 and 3, and minimum intensity for sample 4. In the spectra shown in Figure 10e, only sample 4 presents an absorption peak centered around 520 nm. This corresponds to the visible  $t_2 \rightarrow \pi^*$  metal-to-ligand charge transfer (MLCT) in N3 dye,<sup>[69]</sup> but compared with that of pure N3, the absorption peak is slightly shifted to shorter wavelengths (a blue-shift) due to the electronic coupling between N3 and ZnO. All the other samples show a monotonic increase in the absorption

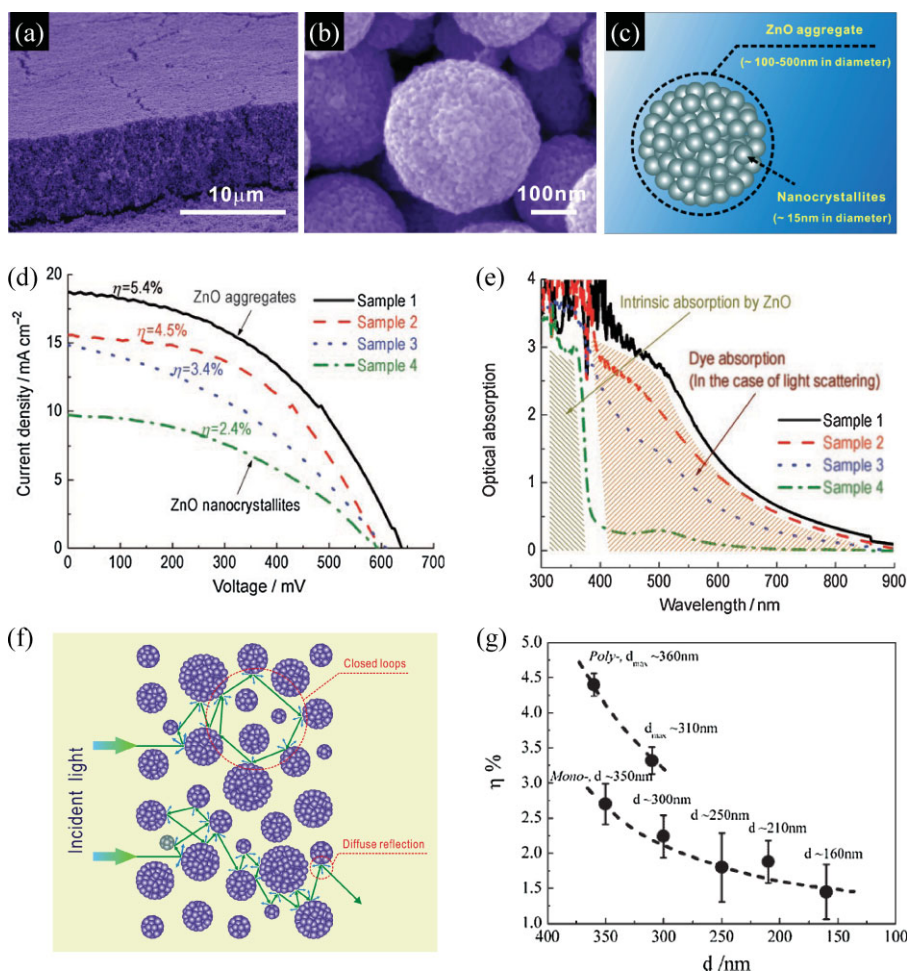


**Figure 10.** ZnO-aggregate dye-sensitized solar cells. a) Cross-sectional SEM image of a ZnO-aggregate film. b) Magnified SEM image of an individual ZnO aggregate. c) Schematic diagram illustrating the microstructure of aggregated ZnO comprised of closely packed nanocrystallites. d) Photovoltaic behavior of N3-dye-adsorbed ZnO-film samples with differences in the degree of aggregation of nanocrystallites. e) Optical absorption spectra for (d). f) Schematic of light scattering and photon localization within a film consisting of submicrometer-sized aggregates. g) Dependence of the overall conversion efficiency on the size and size distribution of aggregates in dye-sensitized ZnO solar cells. Reproduced with permission from [169,170]. Copyright 2008, Wiley-VCH.

intensity as the wavelength varies from visible to ultraviolet. This portion of the absorption is contributed by the dye molecules that are adsorbed on the ZnO surface, and the difference in the absorption intensity implies that the absorption is structure related. It has been suggested that the difference in the absorption of samples 1–3 arises from the submicrometer-sized aggregates that cause the light scattering. This weakens the transmittance of the films and causes pseudo absorption in the spectra. The performance of the solar cell is improved due to the presence of light scattering in hierarchically structured ZnO films, by which the traveling distance of light within the photoelectrode film can be significantly extended (Fig. 10f). As such, the opportunities for incident photons to be captured by the dye molecules are increased. The difference in the optical absorption of the four kinds of film implies that an improvement in the degree of aggregation of nanocrystallites would induce more effective light scattering in the visible region. A photon-localization effect may also occur on these films due to their highly disordered structure that confines the light scattering in closed loops.

Further studies reinforce the light-scattering mechanism. It has been demonstrated that the performance of DSCs with hierarchically structured ZnO films can be significantly affected by either the average size or the size distribution of aggregates.<sup>[170]</sup> The films with polydisperse aggregates, which result in a more disordered structure and achieve better packing, establish higher conversion efficiencies than those with monodisperse aggregates. The enhancement effect becomes more intense when the maximum size of the aggregates in polydisperse films, or the average size of the aggregates in monodisperse films, increases to be as large as, or comparable to, the wavelength of visible light (Fig. 10g). These results confirm the rationality of enhanced solar-cell performance arising from light scattering, generated by hierarchically structured ZnO films and promoting the light-capturing ability of the photoelectrode.

Compared with those using large-sized TiO<sub>2</sub> particles or photonic-crystal layers reported elsewhere,<sup>[162,166,167]</sup> the method using controlled ZnO aggregation of nanocrystallites in DSCs presents obvious advantages in the generation of light scattering, without causing detrimental loss in the internal surface area of the photoelectrode film. That is, the size of these aggregates is on a submicrometer scale comparable to the wavelength of visible light, so that efficient scattering of the incident light would be established within the photoelectrode film and thus extend the traveling distance of photons, leading to increased opportunity for the photons to be absorbed by dye molecules. Meanwhile, the film with aggregates consisting of interconnected nanosized crystallites provides a highly porous structure, ensuring a large specific surface area for dye adsorption, unlike the large-sized TiO<sub>2</sub> particles with solid cores that consume the internal surface area or the photonic-crystal layer that is added to generate light scattering but with increased film thickness as well as electron diffusion length.

## 5.2. One-Dimensional ZnO Nanostructures for Light Scattering

Recently, the enhancement effect of light scattering on DSC performance was also observed in films consisting of one-

dimensional ZnO nanostructures.<sup>[171]</sup> The films were typically fabricated using a spray deposition technique, where 10-nm-diameter ZnO nanoparticles dispersed in 1-butanol were prepared as a precursor. Based on such a precursor, various nanostructures (nanorods, nanoflakes, or nanobelts) had been produced by an electric-field-induced self-assembly process, which could cause dipole–dipole interactions of nanoparticles. Films fabricated through this technique displayed large surface areas. Moreover, it was speculated that these highly disordered structures contributed to the light-harvesting efficiency of the photoelectrodes by causing random multiple light scattering, as well as possible photon localization because of the formation of optical traps. Typically, an overall conversion efficiency of 4.7% was achieved on films with randomly oriented nanorods.

## 6. Limitation on ZnO-Based DSCs

It has been demonstrated that ZnO has approximately the same band gap and band position as TiO<sub>2</sub>. Furthermore, ZnO possesses a high electron mobility, low combination rate, and good crystallization into an abundance of nanostructures. Many efforts have been made on ZnO-based DSCs with either nanocrystalline films or films consisting of various nanostructures that are highly efficient in electron transport and/or photon capture. However, so far, the results obtained for dye-sensitized ZnO solar cells have still shown relatively low overall conversion efficiencies when compared with TiO<sub>2</sub>-based systems. The limited performance in ZnO-based DSCs may be explained by the instability of ZnO in acidic dye (i.e., protons from the dyes cause the dissolution of Zn atoms at ZnO surface, resulting in the formation of excessive Zn<sup>2+</sup>/dye agglomerates) and the slow electron-injection kinetics from dye to ZnO.

### 6.1. Instability of ZnO in Acidic Dyes

#### 6.1.1. Formation of Zn<sup>2+</sup>/Dye Complex

Commercially available dyes such as N3, N719, or “black” dye derived from ruthenium–polypyridine complexes have been widely used as a sensitizer for TiO<sub>2</sub>-based DSCs. The molecules of these dyes have carboxyl groups that connect with TiO<sub>2</sub>. However, direct use of these dyes with ZnO is difficult because the surface structure of the ZnO crystals may be destroyed when they are soaked in an acidic dye solution containing a Ru complex for an extended period of time. By preparing N3-adsorbed ZnO-nanoparticle films and comparing the transient absorption and fluorescence spectra of those films immersed in dye solution for different durations of time, Horiuchi et al. studied the formation of the Zn<sup>2+</sup>/dye-complex layer on ZnO nanoparticle surface.<sup>[172]</sup> They found that such a complex layer could always be observed if the immersion time was longer than 3 h. Below an immersion time of 10 min, no complex was formed. Westermark et al.<sup>[173]</sup> and Chou et al.<sup>[174]</sup> verified that a short sensitization time may be favorable to avoid the formation of Zn<sup>2+</sup>/dye complex. However, the formation of the Zn<sup>2+</sup>/dye complex seems to be very sensitive to the experimental conditions, resulting in a

considerable difference in the optimization of the sensitization time. The  $Zn^{2+}$ /dye complex can agglomerate to form a thick covering layer instead of a monolayer, and is therefore inactive for electron injection. This means that the sensitization time of ZnO in acidic dyes is limited by its stability, resulting in insufficient dye adsorption and electron injection and thus poor performance of DSCs.

The spatial images of both the distribution of dye adsorbed on semiconductor surface and the electron-injection process from an excited dye into nanocrystallites can be reflected by transient absorption microscopy, a newly developed technique for studying heterogeneous photochemical systems.<sup>[175]</sup> A typical example of using transient absorption microscopy for the study of N3-adsorbed ZnO films is based on the experimental observations that (1) ZnO films immersed in dye for an extremely short time (3 min) can obtain an adsorbed monolayer of dye molecules on the surface, whereas a long-time immersion (12 h) leads to serious agglomeration of the  $Zn^{2+}$ /dye complex, (2) the images of ground-state absorption are not homogeneous across the films, revealing that the ground-state absorption is not due solely to N3 dye directly adsorbed on the ZnO surface, but also due to the dye in the agglomerates, (3) fluorescence emission can only be obtained for concentrated N3/ZnO film, instead of diluted N3/ZnO film, indicating that the fluorescence emission originates from the excited  $Zn^{2+}$ /dye agglomerates, which is consistent with the observed heterogeneous image, and (4) the image of transient absorption, in which the intensity is proportional to the efficiency of electron injection, is shown to be homogeneous in the film region. That is, in spite of the heterogeneity of the distribution of  $Zn^{2+}$ /dye agglomerates, the electron injection is distributed homogeneously on the ZnO film. In other words, those  $Zn^{2+}$ /dye agglomerates are inactive for electron injection. Accordingly, a model is proposed to exhibit the structure of dye adsorption on ZnO and the distribution of  $Zn^{2+}$ /dye agglomerates (Fig. 11). With this model, a monolayer of dye molecules is formed homogeneously on the ZnO-nanoparticle surface. These dyes are active and contribute to electron injection. On the exterior of the monolayer, agglomeration of  $Zn^{2+}$ /dye complex is evenly yielded to form micrometer-sized crystals. These agglomerates are inactive since those photogenerated electrons in the agglomerates are separated from the ZnO semiconductor by the layer of active dyes.

The formation of  $Zn^{2+}$ /dye complex has been attributed to the dissolution of surface Zn atoms by the protons released from the dye molecules in an ethanolic solution. The instability of ZnO

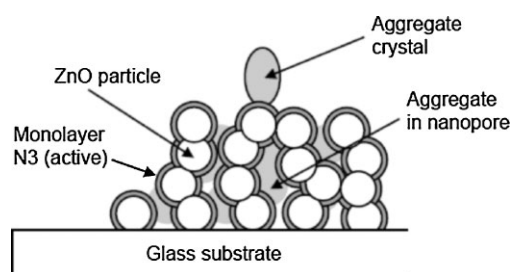


**Figure 11.** Proposed structure of a N3-dye-sensitized ZnO film with  $Zn^{2+}$ /dye agglomerates. Reproduced with permission from [183]. Copyright 2006, American Chemical Society.

results from its surface properties in acidic dyes. In general, in a solution, the surface of the oxide is predominantly positively charged at a pH below the point of zero charge and negatively charged above this value, while the point of zero charge of metal oxides is defined as the pH at which the concentrations of protonated and deprotonated surface groups are equal. For the ZnO sensitization process with Ru-complex dye, the pH (pH = 5) is much lower than the point of zero charge of ZnO ( $\approx 9$ ). That means that the ZnO surface is positively charged. Thus, the protons adsorbed on the ZnO surface will dissolve the ZnO.<sup>[173]</sup> Bahnemann has shown that dissolution of ZnO colloids occurs below pH 7.4.<sup>[176]</sup> Theoretical investigations by Persson et al. also indicate that adsorption of formic acid (HCOOH) on the ZnO (10 $\bar{1}0$ ) surface may increase the bond length between Zn and O atoms, and thus weaken the Zn–O bond, resulting in the dissolution of surface Zn atoms.<sup>[177]</sup> Another recent study reports that temperature may have an effect on the adsorption and aggregation of dye on the surface of ZnO.<sup>[178]</sup> A higher temperature can effectively reduce the occurrence of dye aggregation and increase the amount of dye adsorbed on the ZnO.

### 6.1.2. Coating on ZnO for Improved Stability

In order to avoid the formation of  $Zn^{2+}$ /dye complexes, many core–shell structures have been developed to improve the stability of ZnO in acidic dye solution by coating a buffer layer on the ZnO surface.  $SiO_2$  has been demonstrated to be a very effective shell material on ZnO, preventing the generation of  $Zn^{2+}$ /dye agglomerates due to the strong interaction between  $Si^{4+}$  and  $O^{2-}$  ions. Typically, when 5-nm-diameter ZnO nanoparticles were coated with a  $SiO_2$  layer (molar ratio of Si to Zn around 0.2), for a 13- $\mu m$ -thick film, an overall conversion efficiency of 5.2% was achieved.<sup>[179]</sup> The role of the  $SiO_2$  shell was demonstrated to (1) suppress the formation of  $Zn^{2+}$ /dye agglomerates and establish adequate dye adsorption on the electrode surface, and (2) reduce the recombination sites at ZnO surface.

$TiO_2$  is also a representative material that may be used for the surface modification of ZnO to prevent the surface Zn atoms from being dissolved and forming  $Zn^{2+}$ /dye agglomerates. A simple route for coating a  $TiO_2$  layer on ZnO can be implemented by directly soaking or dip coating ZnO film in a solution of 10 mM titanium alkoxide ( $Ti(OBu)_4$ ) dissolved in 2-propanol, followed by heat treatment at 400 °C.<sup>[180]</sup> It can also be achieved by electrochemical deposition in a solution containing 0.15 M  $LiNO_3$ , 0.005 M  $Zn(NO_3)_2$  hydrate, and 0.05 M  $ZnCl_2$  in propylene carbonate.<sup>[181]</sup> However, these methods are not without their drawbacks on account of the fact that the film thickness is hard to control. ALD is a newly developed technique for thin-film fabrication and has been also reported for coating  $TiO_2$  layers on the surface of nanostructured ZnO.<sup>[182]</sup> With the ALD technique, the growth rate as well as the shell thickness can be precisely controlled on the order of 1 nm. Figure 12 shows typical TEM images of ZnO– $TiO_2$  core–shell nanowires and nanotube-structured  $TiO_2$  shells prepared by the ALD method.<sup>[183]</sup> The crystal phase of the deposited  $TiO_2$  shell has been demonstrated to be dependent on its thickness, being completely amorphous for less than 5 nm and polycrystalline anatase for thicker films. Besides the protection effect of the  $TiO_2$  shell

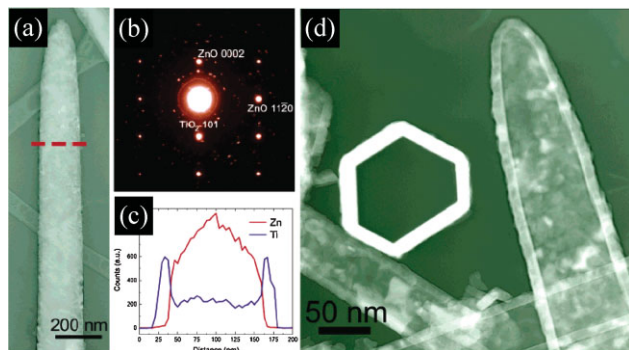


**Figure 12.** Characterization of a ZnO–TiO<sub>2</sub> core-shell-structured nanowire and nanotube-structured TiO<sub>2</sub> shell prepared by ALD. Reproduced with permission from [183] Copyright 2006, American Chemical Society. a) TEM image of a core-shell structure with ZnO-nanowire core and TiO<sub>2</sub> shell. b) Selected-area electron diffraction pattern of the core-shell structured nanowire. c) Energy-dispersive spectroscopy (EDS) elemental profile along the dashed line in (a). d) TEM image of a nanotube-structured TiO<sub>2</sub> shell, where the ZnO-nanowire core was removed using 1 M aqueous HCl.

(which may improve the stability of ZnO nanowires in acidic dye and, therefore, avoid the formation of Zn<sup>2+</sup>/dye agglomerates), the TiO<sub>2</sub> shell is also believed to play a role in suppressing the recombination rate by passivating the recombination sites on the ZnO surface and by forming an energy barrier that prevents the injected electrons from approaching the nanowire surface. As a result, solar cells with TiO<sub>2</sub>-coated ZnO nanowire arrays have demonstrated significant enhancements in both the open-circuit voltage and fill factor, leading to as much as doubly improved overall conversion efficiencies. Typically, it was reported that the overall conversion efficiency was increased from 0.85% for bare ZnO nanowire array to 1.7–2.1% with a crystalline TiO<sub>2</sub> coating layer (10–35 nm thick) on ZnO.<sup>[183]</sup> In a related set of experiments, amorphous Al<sub>2</sub>O<sub>3</sub> was also studied as a coating material on ZnO nanowires. However, in contrast to the case using TiO<sub>2</sub><sup>[183]</sup> or the result reported for ZnO nanoparticles coated with SiO<sub>2</sub>,<sup>[179]</sup> the Al<sub>2</sub>O<sub>3</sub> shell was proven to act as an insulating barrier, leading to a slight increase in the open-circuit voltage ( $V_{OC}$ ) of the cell but a larger decrease in short-circuit current density ( $J_{SC}$ ) with increasing shell thickness and, ultimately, a decrease in the power-conversion efficiency of the solar cells. The increase in  $V_{OC}$  was attributed to the Al<sub>2</sub>O<sub>3</sub> shell having the capacity to passivate the recombination sites on the surface of ZnO nanowires, whereas the decrease in  $J_{SC}$  was because the Al<sub>2</sub>O<sub>3</sub> shell could simultaneously lower or block electron injection at the semiconductor–electrolyte interface.

Although the use of oxides, such as SiO<sub>2</sub>, TiO<sub>2</sub>, and Al<sub>2</sub>O<sub>3</sub>, as shells on ZnO is based on a basic consideration of improving the surface stability of ZnO in acidic dye, the resultant effect on the photovoltaic efficiency by these materials is obviously different. It seems that better insight into how to select the shell material for ZnO and achieve an optimal enhancement of the photovoltaic efficiency is still in need of further investigation. However, in general, it is believed that the surface-modification effect is related to (1) the chemical bonding between O<sup>2-</sup> ions and the cations (i.e., Si<sup>4+</sup>, Ti<sup>4+</sup>, or Al<sup>3+</sup>), which may lead to a difference in interface states and thus affect the electron-injection process, and (2) the methods used for the formation of oxide shells. As mentioned

above, these methods, which can be greatly different, typically include soaking ZnO nanoparticles in tetramethylorthosilicate (TMOS) for the coating of SiO<sub>2</sub> or using the ALD technique for the deposition of a TiO<sub>2</sub> or Al<sub>2</sub>O<sub>3</sub> layer on ZnO nanowires. These processes are likely to result in different qualities of the coating layer in terms of, for example, the crystallinity, the surface roughness, and the coverage density. Furthermore, the enhancement effect is also thought to be related to the morphology of the nanostructures. For example, in the case of ZnO mentioned above, the nanoparticles and nanowire arrays possess different specific surface areas and porosities and, therefore, the dye-diffusion and adsorption dynamics would be different. This would lead to a difference in the degree of photovoltaic-efficiency enhancement after being coated with a SiO<sub>2</sub> or TiO<sub>2</sub> shell.

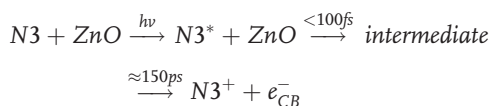
## 6.2. Low Electron-Injection Efficiency

Electron-injection efficiency describes the probability of photo-generated electrons transferring from the dye molecules to semiconductor. In term of DSC performance, the electron injection efficiency,  $\varphi_{inj}$ , and the incident photon-to-current conversion efficiency (IPCE) are related by  $IPCE(\lambda) = L \cdot LHE(\lambda) \times \varphi_{inj} \times \eta_C$ , where  $LHE(\lambda)$  is the light-harvesting efficiency,  $\lambda$  is the wavelength of incident light, and  $\eta_C$  is the collecting efficiency for injected electrons at the back contact.<sup>[69]</sup> The electron-injection efficiency is, above all, determined by the electronic coupling between the dye and semiconductor, and it is also judged by the relative energy levels of the dye and semiconductor, the residential lifetime of photogenerated electrons in the dye molecules, and the density of electron-accepting states in the semiconductor. In particular, for ZnO sensitized with Ru-complex acidic dyes, it has been demonstrated that the injection process may also be influenced by the formation of Zn<sup>2+</sup>/dye-complex agglomerates, resulting in a low electron-injection efficiency.

For either ZnO or TiO<sub>2</sub>, the injection of electrons from Ru-based dyes to a semiconductor shows similar kinetics that include a fast component of less than 100 fs and slower components on a picosecond time scale.<sup>[184–189]</sup> Such biphasic kinetics are caused by competition processes between the ultrafast electron injection and molecular relaxation.<sup>[190]</sup> However, for ZnO with Ru-based dyes, the electron injection is dominated by slow components, whereas for TiO<sub>2</sub> it is dominated by fast components, leading to a difference of more than 100 times in the injection rate constant. Based on a two-state injection model<sup>[186]</sup> and using ultrafast infrared transient absorption spectroscopy, a quantitative study has been given to describe the electron-injection dynamics from Ru–polypyridyl complexes to nanocrystalline ZnO or TiO<sub>2</sub> film, revealing that the injection time scales from unthermalized and relaxed excited states to ZnO are estimated to be 1.5 and 150 ps, respectively, both of which are one order of magnitude slower than those of TiO<sub>2</sub>.<sup>[184]</sup> The different injection dynamics most likely originate from the conduction-band structures of the semiconductors. That is, the ZnO conduction bands are largely derived from the empty s and p orbitals of Zn<sup>2+</sup>, while the TiO<sub>2</sub> conduction band is comprised primarily of empty 3d orbitals from Ti<sup>4+</sup>.<sup>[190]</sup> The difference in band structure results in a different density of states and, possibly, different electronic coupling strengths with the

adsorbate. Enright et al. estimated that the density of conduction-band states near the band edge is as much as two orders of magnitude higher in TiO<sub>2</sub> by reason of the larger effective mass of the conduction-band electron in TiO<sub>2</sub> (5–10*m<sub>e</sub>*) than that in ZnO (*≈*0.3*m<sub>e</sub>*).<sup>[149]</sup>

The slower electron-injection dynamics for ZnO with Ru-based dyes is also proposed to be a result of the electron injection proceeding stepwise via intermediate states, as described by<sup>[191]</sup>



where N3\* and N3<sup>+</sup> represent the excited and oxidized states, respectively, and e<sub>CB</sub><sup>-</sup> indicates a conducting electron in ZnO. The origin of the intermediate states has been ascribed to the interaction between the photoexcited dye and localized surface states on the ZnO surface. The electron transfer is considered to occur slowly due to the existence of intermediate states and therefore results in a low injection efficiency.

### 6.3. New Types of Photosensitizers for ZnO

In view of the instability of ZnO in acidic dyes, the development of new types of photosensitizers for use in ZnO DSCs is a subject that has already been widely investigated. These photosensitizers are expected to be chemically bonded to the ZnO semiconductor, be charge transferable with a high injection efficiency, and be effective for light absorption in a broad wavelength range. New types of dyes have already been developed with the aim of fulfilling these criteria. Examples include heptamethine-cyanine dyes adsorbed on ZnO for absorption in the red/near-infrared (IR) region,<sup>[192,193]</sup> and unsymmetrical squaraine dyes with deoxycholic acid, which increase photovoltage and photocurrent by suppressing electron back transport.<sup>[194]</sup> Mercurochrome (C<sub>20</sub>H<sub>8</sub>Br<sub>2</sub>HgNa<sub>2</sub>O) is one of the newly developed photosensitizers that, to date, is most suitable for ZnO, offering an IPCE as high as 69% at 510 nm and an overall conversion efficiency of 2.5%.<sup>[195,196]</sup> It was also reported that mercurochrome photosensitizer could provide ZnO DSCs with a fill factor significantly larger than that obtained with N3 dye, where the latter device was believed to possess a higher degree of interfacial electron recombination due to the higher surface-trap density in the N3-dye-adsorbed ZnO.<sup>[197]</sup> Eosin Y is also a very efficient dye for ZnO-based DSCs, with 1.11% conversion efficiency for nanocrystalline films.<sup>[66]</sup> When eosin Y is combined with a nanoporous film, overall conversion efficiencies of 2.0–2.4% have been obtained.<sup>[198,199]</sup> Recently, Senevirathne et al. reported that the use of acriflavine (1,6-diamino-10-methylacridinium chloride) as a photosensitizer for ZnO could generate photocurrents that are an order of magnitude higher than in the case of TiO<sub>2</sub>.<sup>[200]</sup>

As an alternative to organic dyes, semiconductor quantum dots have also been studied as photosensitizers for application in DSCs, which are accordingly sometimes called semiconductor-sensitized solar cells (SSCs). Quantum dots take the form of nanocrystals of compound semiconductors and, therefore, offer the advantage of stability over the metallorganic or even pure organic dyes. Moreover, quantum dots present the ability to match the solar spectrum better because their absorption-

wavelength range can be tailored by size quantization. More recently, it was reported that the quantum dots were able to generate multiple electron-hole pairs per photon, which would be greatly beneficial in terms of photovoltaic devices possibly attaining extremely high conversion efficiencies.<sup>[201,202]</sup> Up to now, the highest overall conversion efficiency of TiO<sub>2</sub> sensitized with quantum dots is about 2.8%.<sup>[203,204]</sup> A few attempts have also been made on ZnO. One example is to combine ZnO nanowires with CdSe quantum dots for a photoelectrochemical cell, which has demonstrated an internal quantum efficiency of 50–60%, comparable to the results obtained for similar ZnO nanowires sensitized with Ru-complex dye.<sup>[205]</sup>

## 7. Conclusions

Nanostructures of ZnO have been demonstrated to be advantageous for use as the photoelectrode film in DSCs. To review, these nanostructures can offer larger specific surface areas for dye adsorption than bulk film material, direct pathways for electron transport, and light-scattering effects that extend the traveling distance of light within the photoelectrode film. Core-shell structures, typically with a ZnO shell on a TiO<sub>2</sub> core, are demonstrated for reduced recombination rates. Table 2 summarizes the majority of recent results obtained for DSCs based on ZnO nanostructures. Among these nanostructures, ZnO aggregates feature a structure with aggregation of nanosized crystallites and thus combine a relatively large surface area with efficient light-scattering centers. As a result, ZnO aggregates possess the highest conversion efficiency of 5.4%, which is more than double the 2.4% obtained for dispersed ZnO nanocrystallites. This is a desirable scenario found in ZnO, indicating that the performance of DSCs based on nanoparticulate films can be further improved via the route of aggregates. As such, it would be anticipated that this approach can also work for nanocrystalline TiO<sub>2</sub> films, which have already achieved the maximum conversion efficiency of around 11%.

Actually, there are already quite a few investigations on the use of the light-scattering effect for TiO<sub>2</sub>-based DSCs. The aforementioned methods introduce light scattering by admixing the nanocrystalline film with large-sized TiO<sub>2</sub> particles or by incorporating a photonic-crystal layer. A more frequently reported method is to place a layer of 400-nm TiO<sub>2</sub> particles above the nanocrystalline film, motivating light scattering and reducing the reflection loss of incident light. Typically, the photoelectrode includes a 12–14- $\mu$ m-thick nanocrystalline film and a scattering layer around 2–5- $\mu$ m thick. The scattering layer should be effective in increasing the harvesting of light. However, the disadvantage of such a configuration is that, even though a light-scattering layer is used, the thickness of the nanocrystalline film is still expected to be larger than the light-absorption length ( $\alpha^{-1}$ ,  $\alpha$  is the absorption coefficient). This is so that most of the incident photons can be captured. In this case, recombination is unavoidable and may be very serious since the film thickness is larger than the electron diffusion length. Moreover, the presence of a scattering layer located between the nanocrystalline film and electrolyte is likely to affect the regeneration of the oxidized dye. This is due to the possible reduction in the concentration of redox couples in the electrolyte around the TiO<sub>2</sub> nanoparticles. The situation is very different for the hierarchically structured films

**Table 2.** Summary of DSCs based on ZnO nanostructures.

Structure	Photosensitizer	Efficiency	Ref.	Structure	Photosensitizer	Efficiency	Ref.	
Nanoparticles	N719	0.44%, 2.1% (0.06 sun), 2.22%	[72,77,115]	Nanotips	N719	0.55%, 0.77%	[126,127]	
	N719	5% (0.1 sun)	[73,74]	Nanotubes	N719	1.6%, 2.3%	[124,125]	
	N3	0.4%, 0.75%, 2% (0.56 sun), 3.4%	[67,76,80,93]	Nanobelts	N719	2.6%	[95]	
	heptamethine cyanine	0.16%, 0.67	[192,193]	Nanosheets	N719	2.61%, 3.3%	[91,94]	
	unsymmetrical squaraine	1.5%	[194]		N3	1.55%	[93]	
	eosin-Y	1.11%	[66]	Nanotetrapods	N719	1.20%, 3.27%	[96,97]	
	acriflavine	0.588%	[200]	Nanoflowers	N719	1.9%	[128]	
	mercurochrome	2.5%	[195,196]	Core-shell nanoparticles (ZnO-TiO <sub>2</sub> )	N719	1.78%	[180]	
	Nanoporous films	N3	5.08% (0.53 sun)	[85]	Core-shell nanoparticles (ZnO-SiO <sub>2</sub> )	N719	5.2%	[179]
		N719	3.9%, 4.1%	[88,90]	Core-shell nanoparticles (TiO <sub>2</sub> -ZnO)	N3	4.3%, 4.51%, 9.8%	[135,146,147]
N719		0.23% (hybrid ZnO/N719)	[62]		N719	6.55%	[150]	
D149		4.27%	[92]		N3	1.21% (0.2 sun, flexible substrate)	[144]	
eosin-Y		2.0%, 2.4%	[198,199]	Core-shell nanoporous films (ZnO-TiO <sub>2</sub> )	N719	1.02%	[61]	
eosin-Y		3.31% (0.1 sun)	[198]	Core-shell nanowires (ZnO-TiO <sub>2</sub> )	N719	2.25%	[183]	
Nanowires		N3	0.73%, 2.1%, 2.4%, 4.7%	[113,117,171,197]	Core-shell nanowires (ZnO-Al <sub>2</sub> O <sub>3</sub> )	N719	↓	[183]
		N719	0.3%, 0.6%, 0.9%, 1.5%, 1.54%	[110,115,116,118,119]	Core-shell nanotubes (TiO <sub>2</sub> -ZnO)	N719	0.704%	[181]
	QDs (CdSe)	0.4%	[205]	Aggregates	N3	3.51%, 4.4%, 5.4%	[168-170,174]	
Dendritic nanowires	N719	0.5%, 1.1%	[103,129]					
Nanowire/nanoparticle composite films	N719	0.9% ;(flexible substrate)	[122]					
	Mercurochrome	2.2%	[121]					

with ZnO or TiO<sub>2</sub> aggregates. These films have the capability to generate light scattering within the photoelectrode film so as to enhance the light-harvesting efficiency. In this case, it is possible to use a photoelectrode film with a reduced thickness. The light-absorption length may remain unchanged, or even increase, due to the extended light-traveling distance caused by the light-scattering actions of the aggregates. This would result in a decreased recombination rate so as to benefit the photocurrent density as well as the power-conversion efficiency of a solar cell.

However, when a similar light-management strategy to the ZnO case is employed with TiO<sub>2</sub>, it is hampered by the availability of synthesis methods in the production of appropriate nanostructures. Although the mechanism of growth in ZnO aggregates has been proposed to be a result of the dipole nature of ZnO nanocrystallites in a supersaturation colloidal solution,<sup>[206]</sup> it seems to be unsuitable for TiO<sub>2</sub>. As an outlook, we would like to propose several possible methods that are intended for the synthesis of TiO<sub>2</sub> aggregates, including (1) surface modification of ZnO aggregates using TiO<sub>2</sub>, (2) hydrothermal growth of TiO<sub>2</sub>-nanoparticle aggregates, (3) emulsion-assisted aggregation of TiO<sub>2</sub> nanostructures, (4) electrostatic spray deposition using colloidal TiO<sub>2</sub>, and (5) synthesis of porous-structured TiO<sub>2</sub> spheres.

### 7.1. Surface Modification of ZnO Aggregates – An Indirect Method for TiO<sub>2</sub> Aggregates

The modification of ZnO aggregates with TiO<sub>2</sub> is a task that can be achieved by simply utilizing the already-achieved aggregate structure of ZnO to serve as light scattering centers and, at the same time, attain a TiO<sub>2</sub> surface for dye adsorption. Many physical- or chemical-deposition methods can be used for this purpose. However, the recently developed ALD technique distinguishes itself by offering atomic-level thickness as well as large-area uniformity.<sup>[207]</sup> ALD is actually a self-limiting process of vapor-solid deposition, in which film formation takes place in a cyclic manner through a series of saturated surface reactions between the adsorbed precursor and the species left on the surface, and, moreover, multilayer adsorption is, by definition, excluded. In this method, the film thickness can be precisely controlled by adjusting the number of deposition cycles and growth rate.<sup>[183]</sup> As for the deposition of TiO<sub>2</sub>, many titanium salts, such as titanium chloride (TiCl<sub>4</sub>),<sup>[208]</sup> titanium isopropoxide (Ti(O<sup>i</sup>Pr)<sub>4</sub>),<sup>[209,210]</sup> titanium ethoxide (Ti(OEt)<sub>4</sub>),<sup>[211,212]</sup> and titanium methoxide (Ti(OMe)<sub>4</sub>),<sup>[213]</sup> can be adopted as the titanium-oxide precursor due to the fact that they are liquids and also present a moderate vapor pressure, which is convenient

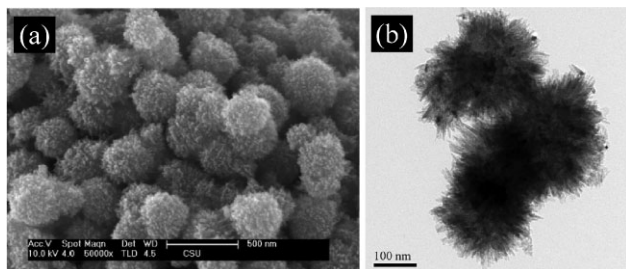


**Figure 13.** The morphology and structure of flower-like TiO<sub>2</sub> nanostructures. Reproduced with permission from [215]. Copyright 2008, Elsevier. a) SEM image of spherical aggregates with an average diameter of  $\approx 300$  nm. b) TEM image revealing that the aggregates consist of needle-like nanoparticles.

to handle. It has been reported that both the crystal structure and phase of TiO<sub>2</sub> are predominately determined by the deposition temperature.<sup>[213]</sup> For example, when using Ti(OMe)<sub>4</sub> as the titanium precursor, TiO<sub>2</sub> films typically deposited at 200 °C are amorphous, whereas those deposited at 250 °C or above are polycrystalline with anatase phase.<sup>[214]</sup>

## 7.2. Hydrothermal Growth of TiO<sub>2</sub> Nanoparticle Aggregates

A recent study reported on the synthesis of flower-like TiO<sub>2</sub> nanostructures by hydrothermal treatment of titanium tetrabutoxide (Ti(OBu)<sub>4</sub>) aqueous solution under strongly acidic conditions.<sup>[215]</sup> These flower-like nanostructures were aggregated by needle-like TiO<sub>2</sub> nanoparticles and possessed a spherical shape with a size of about 300 nm (Fig. 13). These structures appear to be promising as efficient light scatterers for DSCs. The formation of flower-like nanostructures has been ascribed to the hydrolysis of Ti(OBu)<sub>4</sub> with high concentration, which leads to a large amount of needle-like nanoparticles of Ti(OC<sub>4</sub>H<sub>9</sub>)<sub>4-n</sub>(OH)<sub>n</sub>. These nanoparticles are homogeneously adsorbed at the active sites around the surface of TiO<sub>2</sub> nuclei generated at the primary stage of hydrolysis, resulting in radial growth from the center. It was mentioned that a major proportion of the as-synthesized nanostructures were rutile-phase TiO<sub>2</sub> due to the strongly acidic conditions in the presence of Cl<sup>-</sup>.<sup>[216]</sup>

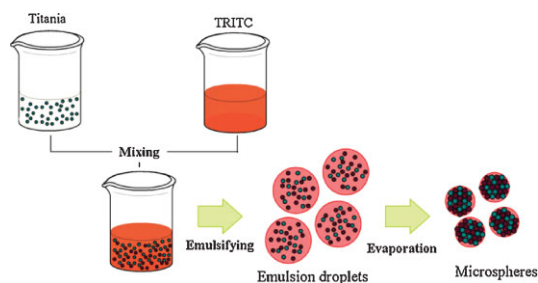


**Figure 14.** Schematic of the emulsion-assisted method for the synthesis of spherical TiO<sub>2</sub> aggregates with nanoparticles. (TRITC = tetramethylrhodamine isothiocyanate). Reproduced with permission from [217]. Copyright 2008, Wiley-VCH.

## 7.3. Emulsion-Assisted Synthesis of TiO<sub>2</sub> Nanostructure Aggregation

Emulsion-assisted synthesis is an easy route towards the creation of colloidal aggregates by means of water-in-oil emulsion droplets. In this technique, the colloidal nanoparticles are encapsulated in water droplets that provide confined geometries. When the water is removed from the droplets by drying, the colloidal nanoparticles spontaneously assemble to form spherical aggregates (Fig. 14).<sup>[217–221]</sup> The size of the aggregates can be readily controlled by tuning the tip size of the micropipette that emulsifies the suspension or changing the weight fraction of nanoparticles in suspension. Kim et al. illustrated the preparation of TiO<sub>2</sub> microspheres by using the emulsion-assisted method.<sup>[217]</sup> It was demonstrated that the size of the microspheres,  $d_m$ , could be estimated by the relation  $d_m \propto d_t \varphi_w^{1/3}$ , where  $d_t$  is the inner diameter of the micropipette, and  $\varphi_w$  is the weight fraction of TiO<sub>2</sub> nanoparticles in suspension.

Compared with other methods of preparing colloidal aggregates, the emulsion-assisted method possesses the advantage that it does not have any requirement towards the properties of the constituent materials provided that they are dispersed in a liquid medium, on the nanometer scale, in a stable manner. The technological importance of this method is its viability for the spherical aggregation of other TiO<sub>2</sub> nanomaterials, such as TiO<sub>2</sub> nanotubes, which exhibit a huge potential for highly efficient DSCs.<sup>[222–224]</sup>

## 7.4. Electrostatic-Spray-Deposition Fabrication of TiO<sub>2</sub> Aggregates

ESD is a process in which a colloidal solution (containing nanoparticles, binder, and solvent) is atomized into charged droplets through a capillary needle by an electrohydrodynamic force and a film is formed on the substrate with heat treatment for solvent evaporation (see Section 2.1.2.).<sup>[80,225]</sup> This technique allows the packaging of nanoparticles into droplets, and the size of the droplets can be adjusted in a wide range from a few nanometers up to hundreds of micrometers. It is, therefore, a promising method that may be employed for the fabrication of TiO<sub>2</sub> aggregates consisting of nanocrystallites.

## 7.5. Synthesis of Porous-Structured TiO<sub>2</sub> Spheres

Porously structured TiO<sub>2</sub> spheres with submicrometer sizes have a structure similar to that of nanocrystallite aggregates, thus enabling efficient light scattering and large surface areas to be attained simultaneously. The synthesis of porous-structured TiO<sub>2</sub> spheres can be achieved using a template-free method via a sol-gel process combined with the inverse miniemulsion technique. In this method, droplets are generated by a dispersed aqueous phase that consists of a precursor material of titania mixed with a continuous organic phase containing surfactants. During hydrolysis and condensation, each droplet acts as a nanoreactor for the encapsulation of colloidal TiO<sub>2</sub>. Unlike conventional emulsion, in which diffusion processes take place and lead to an exchange of reactants, a miniemulsion is stabilized

against diffusion and coalescence so that both the droplet size and size distribution can be well controlled.<sup>[226]</sup> Rossmannith et al. reported on the fabrication of porous-structured TiO<sub>2</sub> by using glycol-modified titanate (bis(2-hydroxyethyl)titanate, EGMT) as the precursor material and an amphiphilic block copolymer (P(E/B-b-EO)) as the surfactant.<sup>[227]</sup> The size of the synthesized TiO<sub>2</sub> spheres is typically about 200 nm in diameter. Impressively, these spheres are formed by interconnected nanocrystallites with the size of several nanometers, leading to a high specific surface area of more than 300 m<sup>2</sup> g<sup>-1</sup>.

## Acknowledgements

This work is supported in part by US Department of Energy (DE-FG02-07ER46467), Air Force Office of Scientific Research (AFOSR-MURI, FA9550-06-1-0326), and National Science Foundation (DMI-0455994 and DMR-0605159). This research is also supported by Washington Research Foundation, Washington Technology Center, National Center for Nanomaterials Technology (Korea). Intel Corporation, and EnerG2.

Received: December 25, 2008

Published online: July 6, 2009

- [1] J. Liu, G. Z. Cao, Z. Yang, D. Wang, D. Dubois, X. Zhou, G. L. Graff, L. R. Pederson, J.-G. Zhang, *Chem. Sus. Chem.* **2008**, *1*, 22.
- [2] A. Goetzberger, C. Hebling, *Sol. Energ. Mat. Sol. C* **2000**, *62*, 1.
- [3] A. Goetzberger, C. Hebling, H. W. Schock, *Mater. Sci. Eng. R. Rep.* **2003**, *40*, 1.
- [4] D. M. Bagnall, M. Boreland, *Energ. Pol.* **2008**, *36*, 4390.
- [5] M. A. Green, *Sol. Energ.* **2004**, *76*, 3.
- [6] M. Oliver, T. Jackson, *Energ. Pol.* **1999**, *27*, 371.
- [7] D. M. Chapin, C. S. Fuller, G. L. Pearson, *J. Appl. Phys.* **1954**, *25*, 676.
- [8] K. L. Chopra, P. D. Paulson, V. Dutta, *Prog. Photovoltaics* **2004**, *12*, 69.
- [9] R. B. Bergmann, *Appl. Phys. A* **1999**, *69*, 187.
- [10] A. Shah, P. Torres, R. Tscharnner, N. Wyrsh, H. Keppner, *Science* **1999**, *285*, 692.
- [11] D. E. Carlson, C. R. Wronski, *Appl. Phys. Lett.* **1976**, *28*, 671.
- [12] J. Yang, A. Banerjee, S. Guha, *Sol. Energ. Mat. Sol. C* **2003**, *78*, 597.
- [13] P. Sana, J. Salami, A. Rohatgi, *IEEE Trans. Electron Devices* **1993**, *40*, 1461.
- [14] A. Rohatgi, S. Narasimha, S. Kamra, C. P. Khattak, *IEEE Electron Device Lett.* **1996**, *17*, 401.
- [15] S. Narasimha, A. Rohatgi, *IEEE Trans. Electron Devices* **1998**, *45*, 1776.
- [16] J. S. Ward, K. Ramanathan, F. S. Hasoon, T. J. Coutts, J. Keane, M. A. Contreras, T. Moriarty, R. Noufi, *Prog. Photovoltaics* **2002**, *10*, 41.
- [17] M. Afzaal, P. O'Brien, *J. Mater. Chem.* **2006**, *16*, 1597.
- [18] H. W. Schock, *Appl. Surf. Sci.* **1996**, *92*, 606.
- [19] R. W. Birkmire, *Sol. Energ. Mat. Sol. C* **2001**, *65*, 17.
- [20] M. Gratzel, *Nature* **2001**, *414*, 338.
- [21] J. Bisquert, D. Cahen, G. Hodes, S. Ruhle, A. Zaban, *J. Phys. Chem. B* **2004**, *108*, 8106.
- [22] J. M. Kroon, N. J. Bakker, H. J. P. Smit, P. Liska, K. R. Thampi, P. Wang, S. M. Zakeeruddin, M. Gratzel, A. Hinsch, S. Hore, U. Wurfel, R. Sastrawan, J. R. Durrant, E. Palomares, H. Pettersson, T. Gruszeczi, J. Walter, K. Skupien, G. E. Tulloch, *Prog. Photovoltaics* **2007**, *15*, 1.
- [23] C. Longo, M. A. De Paoli, *J. Braz. Chem. Soc.* **2003**, *14*, 889.
- [24] A. B. F. Martinson, T. W. Hamann, M. J. Pellin, J. T. Hupp, *Chem. Eur. J.* **2008**, *14*, 4458.
- [25] M. Gratzel, *Prog. Photovoltaics* **2000**, *8*, 171.
- [26] B. Oregan, M. Gratzel, *Nature* **1991**, *353*, 737.
- [27] M. K. Nazeeruddin, P. Pechy, T. Renouard, S. M. Zakeeruddin, R. Humphry-Baker, P. Comte, P. Liska, L. Cevey, E. Costa, V. Shklover, L. Spiccia, G. B. Deacon, C. A. Bignozzi, M. Gratzel, *J. Am. Chem. Soc.* **2001**, *123*, 1613.
- [28] M. Gratzel, *J. Photochem. Photobiol. C* **2003**, *4*, 145.
- [29] M. Gratzel, *Phil. Trans. Math. Phys. Eng. Sci.* **2007**, *365*, 993.
- [30] J. Nelson, R. E. Chandler, *Coord. Chem. Rev.* **2004**, *248*, 1181.
- [31] J. Nissfolk, K. Fredin, A. Hagfeldt, G. Boschloo, *J. Phys. Chem. B* **2006**, *110*, 17715.
- [32] M. Gratzel, *Inorg. Chem.* **2005**, *44*, 6841.
- [33] M. Gratzel, *J. Photochem. Photobiol. A* **2004**, *164*, 3.
- [34] Z. L. Wang, *J. Phys. Condens. Matter* **2004**, *16*, R829.
- [35] L. Schmidt-Mende, J. L. MacManus-Driscoll, *Mater. Today* **2007**, *10*, 40.
- [36] J. Tornow, K. Schwarzburg, *J. Phys. Chem. C* **2007**, *111*, 8692.
- [37] A. B. Djurisic, Y. H. Leung, *Small* **2006**, *2*, 944.
- [38] U. Pal, J. G. Serrano, P. Santiago, G. Xiong, K. B. Ucer, R. T. Williams, *Opt. Mater.* **2006**, *29*, 65.
- [39] M. L. Curri, R. Comparelli, P. D. Cozzoli, G. Mascolo, A. Agostiano, *Mater. Sci. Eng. C* **2003**, *23*, 285.
- [40] J. Bandara, K. Tennakone, P. P. B. Jayatilaka, *Chemosphere* **2002**, *49*, 439.
- [41] J. Tornow, K. Ellmer, J. Szarko, K. Schwarzburg, *Thin Solid Films* **2008**, *516*, 7139.
- [42] U. Ozgur, Y. I. Alivov, C. Liu, A. Teke, M. A. Reshchikov, S. Dogan, V. Avrutin, S. J. Cho, H. Morkoc, *J. Appl. Phys.* **2005**, *98*, 041301.
- [43] H. Tang, K. Prasad, R. Sanjines, P. E. Schmid, F. Levy, *J. Appl. Phys.* **1994**, *75*, 2042.
- [44] G. Oskam, Z. S. Hu, R. L. Penn, N. Pesika, P. C. Searson, *Phys. Rev. E* **2002**, *66*, 011403.
- [45] H. S. Bae, M. H. Yoon, J. H. Kim, S. Im, *Appl. Phys. Lett.* **2003**, *83*, 5313.
- [46] K. Keis, A. Roos, *Opt. Mater.* **2002**, *20*, 35.
- [47] V. Noack, H. Weller, A. Eychmuller, *J. Phys. Chem. B* **2002**, *106*, 8514.
- [48] J. J. Wu, G. R. Chen, C. C. Lu, W. T. Wu, J. S. Chen, *Nanotechnology* **2008**, *19*, 105702.
- [49] A. S. Arico, P. Bruce, B. Scrosati, J. M. Tarascon, W. Van Schalkwijk, *Nat. Mater.* **2005**, *4*, 366.
- [50] Y. N. Xia, P. D. Yang, Y. G. Sun, Y. Y. Wu, B. Mayers, B. Gates, Y. D. Yin, F. Kim, Y. Q. Yan, *Adv. Mater.* **2003**, *15*, 353.
- [51] K. Bittkau, R. Carius, *Superlatt. Microstruct.* **2007**, *42*, 47.
- [52] E. A. Meulenkaamp, *J. Phys. Chem. B* **1998**, *102*, 5566.
- [53] M. Vafae, M. S. Ghamsari, *Mater. Lett.* **2007**, *61*, 3265.
- [54] S. Kar, A. Dev, S. Chaudhuri, *J. Phys. Chem. B* **2006**, *110*, 17848.
- [55] P. D. Yang, H. Q. Yan, S. Mao, R. Russo, J. Johnson, R. Saykally, N. Morris, J. Pham, R. R. He, H. J. Choi, *Adv. Funct. Mater.* **2002**, *12*, 323.
- [56] Q. C. Li, V. Kumar, Y. Li, H. T. Zhang, T. J. Marks, R. P. H. Chang, *Chem. Mater.* **2005**, *17*, 1001.
- [57] X. D. Wang, Y. Ding, C. J. Summers, Z. L. Wang, *J. Phys. Chem. B* **2004**, *108*, 8773.
- [58] M. Fu, J. Zhou, Q. F. Xiao, B. Li, R. L. Zong, W. Chen, J. Zhang, *Adv. Mater.* **2006**, *18*, 1001.
- [59] M. Wang, C. H. Ye, Y. Zhang, G. M. Hua, H. X. Wang, M. G. Kong, L. D. Zhang, *J. Cryst. Growth* **2006**, *291*, 334.
- [60] H. H. Wang, C. S. Xie, *J. Cryst. Growth* **2006**, *291*, 187.
- [61] Y. Y. Xi, Y. F. Hsu, A. B. Djurisic, W. K. Chan, *J. Electrochem. Soc.* **2008**, *155*, D595.
- [62] K. Nonomura, T. Yoshida, D. Schlettwein, H. Minoura, *Electrochim. Acta* **2003**, *48*, 3071.
- [63] *Nanoparticle Technology Handbook* (Eds: M. Hosokawa, K. Nogi, M. Naito, T. Yokoyama), Elsevier, Amsterdam **2007**.
- [64] L. Spanhel, M. A. Anderson, *J. Am. Chem. Soc.* **1991**, *113*, 2826.
- [65] K. Keis, L. Vayssieres, H. Rensmo, S. E. Lindquist, A. Hagfeldt, *J. Electrochem. Soc.* **2001**, *148*, A149.
- [66] S. Rani, P. Suri, P. K. Shishodia, R. M. Mehra, *Sol. Energ. Mat. Sol. C* **2008**, *92*, 1639.
- [67] G. Redmond, D. Fitzmaurice, M. Graetzel, *Chem. Mater.* **1994**, *6*, 686.

- [68] A. I. Kontos, A. G. Kontos, D. S. Tsoukleris, M. C. Bernard, N. Spyrellis, P. Falaras, *J. Mater. Process. Technol.* **2008**, 196, 243.
- [69] M. K. Nazeeruddin, A. Kay, I. Rodicio, R. Humphrybaker, E. Muller, P. Liska, N. Vlachopoulos, M. Gratzel, *J. Am. Chem. Soc.* **1993**, 115, 6382.
- [70] M. K. Nazeeruddin, S. M. Zakeeruddin, R. Humphry-Baker, M. Jirousek, P. Liska, N. Vlachopoulos, V. Shklover, C. H. Fischer, M. Gratzel, *Inorg. Chem.* **1999**, 38, 6298.
- [71] M. K. Nazeeruddin, P. Pechy, M. Gratzel, *Chem. Commun.* **1997**, 1705.
- [72] L. Y. Zeng, S. Y. Dai, W. W. Xu, K. J. Wang, *Plasma Sci. Tech.* **2006**, 8, 172.
- [73] K. Keis, C. Bauer, G. Boschloo, A. Hagfeldt, K. Westermark, H. Rensmo, H. Siegbahn, *J. Photochem. Photobiol. A* **2002**, 148, 57.
- [74] K. Keis, E. Magnusson, H. Lindstrom, S. E. Lindquist, A. Hagfeldt, *Sol. Energ. Mat. Sol. C* **2002**, 73, 51.
- [75] Note that the employed illumination intensity in this work is  $10 \text{ mW cm}^{-2}$ , which is one tenth of the standard intensity of  $100 \text{ mW cm}^{-2}$  conventionally used elsewhere. A weaker illumination may result in a slightly boosted conversion efficiency.
- [76] H. Rensmo, K. Keis, H. Lindstrom, S. Sodergren, A. Solbrand, A. Hagfeldt, S. E. Lindquist, L. N. Wang, M. Muhammed, *J. Phys. Chem. B* **1997**, 101, 2598.
- [77] K. Keis, J. Lindgren, S. E. Lindquist, A. Hagfeldt, *Langmuir* **2000**, 16, 4688.
- [78] S. Leeuwenburgh, J. Wolke, J. Schoonman, J. Jansen, *J. Biomed. Mater. Res. A* **2003**, 66A, 330.
- [79] M. C. Siebers, X. F. Walboomers, S. C. G. Leeuwenburgh, J. G. C. Wolke, J. A. Jansen, *Biomaterials* **2004**, 25, 2019.
- [80] X. Sheng, Y. Zhao, J. Zhai, L. Jiang, D. Zhu, *Appl. Phys. A* **2007**, 87, 715.
- [81] M. Y. Song, D. K. Kim, K. J. Ihn, S. M. Jo, D. Y. Kim, *Nanotechnology* **2004**, 15, 1861.
- [82] R. Jose, A. Kumar, V. Thavasi, S. Ramakrishna, *Nanotechnology* **2008**, 19, 424004.
- [83] P. K. Basu, N. Saha, S. Maji, H. Saha, S. Basu, *J. Mater. Sci. Mater. Electron.* **2008**, 19, 493.
- [84] B. Pal, M. Sharon, *Mater. Chem. Phys.* **2002**, 76, 82.
- [85] Z. G. Chen, Y. W. Tang, L. S. Zhang, L. J. Luo, *Electrochim. Acta* **2006**, 51, 5870.
- [86] T. P. Niesen, M. R. De Guire, *J. Electroceram.* **2001**, 6, 169.
- [87] K. Kakiuchi, E. Hosono, T. Kimura, H. Imai, S. Fujihara, *J. Sol-Gel Sci. Technol.* **2006**, 39, 63.
- [88] E. Hosono, S. Fujihara, I. Honna, H. S. Zhou, *Adv. Mater.* **2005**, 17, 2091.
- [89] E. Hosono, S. Fujihara, T. Kimura, H. Imai, *J. Colloid Interface Sci.* **2004**, 272, 391.
- [90] K. Kakiuchi, E. Hosono, S. Fujihara, *J. Photochem. Photobiol. A* **2006**, 179, 81.
- [91] K. Kakiuchi, M. Saito, S. Fujihara, *Thin Solid Films* **2008**, 516, 2026.
- [92] E. Hosono, Y. Mitsui, H. S. Zhou, *Dalton Trans.* **2008**, 5439.
- [93] A. E. Suliman, Y. W. Tang, L. Xu, *Sol. Energ. Mat. Sol. C* **2007**, 91, 1658.
- [94] M. S. Akhtar, M. A. Khan, M. S. Jeon, O. B. Yang, *Electrochim. Acta* **2008**, 53, 7869.
- [95] C. F. Lin, H. Lin, J. B. Li, X. Li, *J. Alloys Compd.* **2008**, 462, 175.
- [96] Y. F. Hsu, Y. Y. Xi, C. T. Yip, A. B. Djurisic, W. K. Chan, *J. Appl. Phys.* **2008**, 103, 083114.
- [97] W. Chen, H. F. Zhang, I. M. Hsing, S. H. Yang, *Electrochem. Commun.* **2009**, 11, 1057.
- [98] H. Q. Yan, R. R. He, J. Pham, P. D. Yang, *Adv. Mater.* **2003**, 15, 402.
- [99] K. D. Benkstein, N. Kopidakis, J. van de Lagemaat, A. J. Frank, *J. Phys. Chem. B* **2003**, 107, 7759.
- [100] A. Hagfeldt, M. Gratzel, *Chem. Rev.* **1995**, 95, 49.
- [101] H. J. Snaith, A. J. Moule, C. Klein, K. Meerholz, R. H. Friend, M. Gratzel, *Nano Lett.* **2007**, 7, 3372.
- [102] K. H. Yu, J. H. Chen, *Nano. Res. Lett.* **2009**, 4, 1.
- [103] J. B. Baxter, E. S. Aydil, *Sol. Energ. Mat. Sol. C* **2006**, 90, 607.
- [104] W. Lee, M. C. Jeong, J. M. Myoung, *Acta Mater.* **2004**, 52, 3949.
- [105] A. Umar, B. K. Kim, J. J. Kim, Y. B. Hahn, *Nanotechnology* **2007**, 18, 175606.
- [106] Y. Tak, K. J. Yong, *J. Phys. Chem. B* **2005**, 109, 19263.
- [107] J. Cembrero, A. Elmanouni, B. Hartiti, M. Mollar, B. Mari, *Thin Solid Films* **2004**, 451, 198.
- [108] C. H. Liu, J. A. Zapien, Y. Yao, X. M. Meng, C. S. Lee, S. S. Fan, Y. Lifshitz, S. T. Lee, *Adv. Mater.* **2003**, 15, 838.
- [109] M. Krunks, A. Katerski, T. Dedova, I. O. Acik, A. Mere, *Sol. Energ. Mat. Sol. C* **2008**, 92, 1016.
- [110] M. Law, L. E. Greene, J. C. Johnson, R. Saykally, P. D. Yang, *Nat. Mater.* **2005**, 4, 455.
- [111] L. E. Greene, B. D. Yuhas, M. Law, D. Zitoun, P. D. Yang, *Inorg. Chem.* **2006**, 45, 7535.
- [112] N. Kopidakis, K. D. Benkstein, J. van de Lagemaat, A. J. Frank, *J. Phys. Chem. B* **2003**, 107, 11307.
- [113] M. Guo, P. Diao, S. M. Cai, *Appl. Surf. Sci.* **2005**, 249, 71.
- [114] J. H. Noh, S. H. Lee, S. Lee, H. S. Jung, *Electron. Mater. Lett.* **2008**, 4, 71.
- [115] K. S. Kim, Y. S. Kang, J. H. Lee, Y. J. Shin, N. G. Park, K. S. Ryu, S. H. Chang, *Bull. Korean Chem. Soc.* **2006**, 27, 295.
- [116] J. B. Baxter, A. M. Walker, K. van Ommering, E. S. Aydil, *Nanotechnology* **2006**, 17, S304.
- [117] M. Guo, P. Diao, X. D. Wang, S. M. Cai, *J. Solid State Chem.* **2005**, 178, 3210.
- [118] A. J. Cheng, Y. H. Tzeng, Y. Zhou, M. Park, T. H. Wu, C. Shannon, D. Wang, W. W. Lee, *Appl. Phys. Lett.* **2008**, 92, 092113.
- [119] R. Zhang, S. Kumar, S. Zou, L. L. Kerr, *Cryst. Growth Des.* **2008**, 8, 381.
- [120] Y. F. Gao, M. Nagai, T. C. Chang, J. J. Shyue, *Cryst. Growth Des.* **2007**, 7, 2467.
- [121] C. H. Ku, J. J. Wu, *Appl. Phys. Lett.* **2007**, 91, 093117.
- [122] C. Y. Jiang, X. W. Sun, K. W. Tan, G. Q. Lo, A. K. K. Kyaw, D. L. Kwong, *Appl. Phys. Lett.* **2008**, 92, 143101.
- [123] L. Vayssieres, K. Keis, A. Hagfeldt, S. E. Lindquist, *Chem. Mater.* **2001**, 13, 4395.
- [124] M. Guo, P. Diao, S. M. Cai, *Chin. Chem. Lett.* **2004**, 15, 1113.
- [125] A. B. F. Martinson, J. W. Elam, J. T. Hupp, M. J. Pellin, *Nano Lett.* **2007**, 7, 2183.
- [126] A. Du Pasquier, H. H. Chen, Y. C. Lu, *Appl. Phys. Lett.* **2006**, 89, 253513.
- [127] H. H. Chen, A. Du Pasquier, G. Saraf, J. Zhong, Y. Lu, *Semicond. Sci. Technol.* **2008**, 23, 045004.
- [128] C. Y. Jiang, X. W. Sun, G. Q. Lo, D. L. Kwong, J. X. Wang, *Appl. Phys. Lett.* **2007**, 90, 263501.
- [129] J. B. Baxter, E. S. Aydil, *Appl. Phys. Lett.* **2005**, 86, 053114.
- [130] N. G. Park, M. G. Kang, K. M. Kim, K. S. Ryu, S. H. Chang, D. K. Kim, J. van de Lagemaat, K. D. Benkstein, A. J. Frank, *Langmuir* **2004**, 20, 4246.
- [131] Y. Diamant, S. Chappel, S. G. Chen, O. Melamed, A. Zaban, *Coord. Chem. Rev.* **2004**, 248, 1271.
- [132] D. B. Menzies, Q. Dai, L. Bourgeois, R. A. Caruso, Y. B. Cheng, G. P. Simon, L. Spiccia, *Nanotechnology* **2007**, 18, 125608.
- [133] J. C. Guo, C. X. She, T. Q. Lian, *J. Phys. Chem. C* **2007**, 111, 8979.
- [134] S. G. Chen, S. Chappel, Y. Diamant, A. Zaban, *Chem. Mater.* **2001**, 13, 4629.
- [135] Z. S. Wang, C. H. Huang, Y. Y. Huang, Y. J. Hou, P. H. Xie, B. W. Zhang, H. M. Cheng, *Chem. Mater.* **2001**, 13, 678.
- [136] K. Tennakone, P. V. V. Jayaweera, P. K. M. Bandaranayake, *J. Photochem. Photobiol. A* **2003**, 158, 125.
- [137] Y. Diamant, S. G. Chen, O. Melamed, A. Zaban, *J. Phys. Chem. B* **2003**, 107, 1977.
- [138] E. Palomares, J. N. Clifford, S. A. Haque, T. Lutz, J. R. Durrant, *J. Am. Chem. Soc.* **2003**, 125, 475.
- [139] N. Okada, S. Karuppuchamy, M. Kurihara, *Chem. Lett.* **2005**, 34, 16.
- [140] Z. S. Wang, M. Yanagida, K. Sayama, H. Sugihara, *Chem. Mater.* **2006**, 18, 2912.

- [141] P. Cheng, C. S. Deng, X. M. Dai, B. Li, D. N. Liu, J. M. Xu, *J. Photochem. Photobiol. A* **2008**, *195*, 144.
- [142] S. Wu, H. W. Han, Q. D. Tai, J. Zhang, S. Xu, C. H. Zhou, Y. Yang, H. Hu, B. L. Chen, B. Sebo, X. Z. Zhao, *Nanotechnology* **2008**, *19*, 215704.
- [143] S. J. Wu, H. W. Han, Q. D. Tai, J. Zhang, S. Xu, C. H. Zhou, Y. Yang, H. Hu, B. L. Chen, X. Z. Zhao, *J. Power Sources* **2008**, *182*, 119.
- [144] S. S. Kim, J. H. Yum, Y. E. Sung, *J. Photochem. Photobiol. A* **2005**, *171*, 269.
- [145] R. S. Mane, W. J. Lee, H. M. Pathan, S. H. Han, *J. Phys. Chem. B* **2005**, *109*, 24254.
- [146] K. E. Kim, S. R. Jang, J. Park, R. Vittal, K. J. Kim, *Sol. Energ. Mat. Sol. C* **2007**, *91*, 366.
- [147] S. J. Roh, R. S. Mane, S. K. Min, W. J. Lee, C. D. Lokhande, S. H. Han, *Appl. Phys. Lett.* **2006**, *89*, 253512.
- [148] K. Tennakone, J. Bandara, P. K. M. Bandaranayake, G. R. A. Kumara, A. Konno, *Jpn. J. Appl. Phys. Part 2* **2001**, *40*, L732.
- [149] B. Enright, D. Fitzmaurice, *J. Phys. Chem.* **1996**, *100*, 1027.
- [150] S. J. Wu, H. W. Han, Q. D. Tai, J. Zhang, B. L. Chen, S. Xu, C. H. Zhou, Y. Yang, H. Hu, X. Z. Zhao, *Appl. Phys. Lett.* **2008**, *92*, 122106.
- [151] J. Bandara, H. C. Weerasinghe, *Sol. Energ. Mat. Sol. C* **2005**, *88*, 341.
- [152] A. Solbrand, K. Keis, S. Sodergren, H. Lindstrom, S. E. Lindquist, A. Hagfeldt, *Sol. Energ. Mat. Sol. C* **2000**, *60*, 181.
- [153] A. Solbrand, H. Lindstrom, H. Rensmo, A. Hagfeldt, S. E. Lindquist, S. Sodergren, *J. Phys. Chem. B* **1997**, *101*, 2514.
- [154] G. Rothenberger, D. Fitzmaurice, M. Gratzel, *J. Phys. Chem.* **1992**, *96*, 5983.
- [155] K. M. P. Bandaranayake, M. K. I. Senevirathna, P. Weligamuwa, K. Tennakone, *Coord. Chem. Rev.* **2004**, *248*, 1277.
- [156] C. Rockstuhl, F. Lederer, K. Bittkau, R. Carius, *Appl. Phys. Lett.* **2007**, *91*, 171104.
- [157] A. Usami, *Chem. Phys. Lett.* **1997**, *277*, 105.
- [158] J. Ferber, J. Luther, *Sol. Energ. Mat. Sol. C* **1998**, *54*, 265.
- [159] G. Rothenberger, P. Comte, M. Gratzel, *Sol. Energ. Mat. Sol. C* **1999**, *58*, 321.
- [160] H. J. Koo, J. Park, B. Yoo, K. Yoo, K. Kim, N. G. Park, *Inorg. Chim. Acta* **2008**, *361*, 677.
- [161] C. Anderson, A. J. Bard, *J. Phys. Chem. B* **1997**, *101*, 2611.
- [162] C. J. Barbe, F. Arendse, P. Comte, M. Jirousek, F. Lenzmann, V. Shklover, M. Gratzel, *J. Am. Ceram. Soc.* **1997**, *80*, 3157.
- [163] S. Hore, P. Nitz, C. Vetter, C. Prah, M. Niggemann, R. Kern, *Chem. Commun.* **2005**, *15*, 2011.
- [164] W. W. So, K. J. Kim, J. K. Lee, S. J. Moon, *Jpn. J. Appl. Phys. Part 1* **2004**, *43*, 1231.
- [165] L. Yang, Y. Lin, J. G. Jia, X. R. Xiao, X. P. Li, X. W. Zhou, *J. Power Sources* **2008**, *182*, 370.
- [166] S. Nishimura, N. Abrams, B. A. Lewis, L. I. Halaoui, T. E. Mallouk, K. D. Benkstein, J. van de Lagemaat, A. J. Frank, *J. Am. Chem. Soc.* **2003**, *125*, 6306.
- [167] L. I. Halaoui, N. M. Abrams, T. E. Mallouk, *J. Phys. Chem. B* **2005**, *109*, 6334.
- [168] T. P. Chou, Q. F. Zhang, G. E. Fryxell, G. Z. Cao, *Adv. Mater.* **2007**, *19*, 2588.
- [169] Q. F. Zhang, T. R. Chou, B. Russo, S. A. Jenekhe, G. Z. Cao, *Angew. Chem. Int. Ed.* **2008**, *47*, 2402.
- [170] Q. F. Zhang, T. P. Chou, B. Russo, S. A. Jenekhe, G. Z. Cao, *Adv. Funct. Mater.* **2008**, *18*, 1654.
- [171] A. R. Rao, V. Dutta, *Nanotechnology* **2008**, *19*, 445712.
- [172] H. Horiuchi, R. Katoh, K. Hara, M. Yanagida, S. Murata, H. Arakawa, M. Tachiya, *J. Phys. Chem. B* **2003**, *107*, 2570.
- [173] K. Westermark, H. Rensmo, H. Siegbahn, K. Keis, A. Hagfeldt, L. Ojamae, P. Persson, *J. Phys. Chem. B* **2002**, *106*, 10102.
- [174] T. P. Chou, Q. F. Zhang, G. Z. Cao, *J. Phys. Chem. C* **2007**, *111*, 18804.
- [175] R. Katoh, A. Furube, Y. Tamaki, T. Yoshihara, M. Murai, K. Hara, S. Murata, H. Arakawa, M. Tachiya, *J. Photochem. Photobiol. A* **2004**, *166*, 69.
- [176] D. W. Bahnemann, *Isr. J. Chem.* **1993**, *33*, 115.
- [177] P. Persson, L. Ojamae, *Chem. Phys. Lett.* **2000**, *321*, 302.
- [178] R. Zhang, J. Pan, E. P. Briggs, M. Thrash, L. L. Kerr, *Sol. Energ. Mat. Sol. C* **2008**, *92*, 425.
- [179] Y. J. Shin, J. H. Lee, J. H. Park, N. G. Park, *Chem. Lett.* **2007**, *36*, 1506.
- [180] Y. J. Shin, K. S. Kim, N. G. Park, K. S. Ryu, S. H. Chang, *Bull. Korean Chem. Soc.* **2005**, *26*, 1929.
- [181] S. H. Kang, J. Y. Kim, Y. Kim, H. S. Kim, Y. E. Sung, *J. Phys. Chem. C* **2007**, *111*, 9614.
- [182] L. E. Greene, M. Law, B. D. Yuhas, P. D. Yang, *J. Phys. Chem. C* **2007**, *111*, 18451.
- [183] M. Law, L. E. Greene, A. Radenovic, T. Kuykendall, J. Liphardt, P. D. Yang, *J. Phys. Chem. B* **2006**, *110*, 22652.
- [184] N. A. Anderson, X. Ai, T. Q. Lian, *J. Phys. Chem. B* **2003**, *107*, 14414.
- [185] J. B. Asbury, E. Hao, Y. Q. Wang, H. N. Ghosh, T. Q. Lian, *J. Phys. Chem. B* **2001**, *105*, 4545.
- [186] J. B. Asbury, N. A. Anderson, E. C. Hao, X. Ai, T. Q. Lian, *J. Phys. Chem. B* **2003**, *107*, 7376.
- [187] D. Kuciauskas, J. E. Monat, R. Villahermosa, H. B. Gray, N. S. Lewis, J. K. McCusker, *J. Phys. Chem. B* **2002**, *106*, 9347.
- [188] G. Benko, J. Kallioinen, J. E. I. Korppi-Tommola, A. P. Yartsev, V. Sundstrom, *J. Am. Chem. Soc.* **2002**, *124*, 489.
- [189] J. B. Asbury, Y. Q. Wang, T. Q. Lian, *J. Phys. Chem. B* **1999**, *103*, 6643.
- [190] N. A. Anderson, T. Lian, *Coord. Chem. Rev.* **2004**, *248*, 1231.
- [191] A. Furube, R. Katoh, K. Hara, S. Murata, H. Arakawa, M. Tachiya, *J. Phys. Chem. B* **2003**, *107*, 4162.
- [192] M. Matsui, Y. Hashimoto, K. Funabiki, J. Y. Jin, T. Yoshida, H. Minoura, *Synth. Met.* **2005**, *148*, 147.
- [193] A. Otsuka, K. Funabiki, N. Sugiyama, H. Mase, T. Yoshida, H. Minoura, M. Matsui, *Chem. Lett.* **2008**, *37*, 176.
- [194] A. Otsuka, K. Funabiki, N. Sugiyama, T. Yoshida, *Chem. Lett.* **2006**, *35*, 666.
- [195] K. Hara, T. Horiguchi, T. Kinoshita, K. Sayama, H. Sugihara, H. Arakawa, *Chem. Lett.* **2000**, 316.
- [196] K. Hara, T. Horiguchi, T. Kinoshita, K. Sayama, H. Sugihara, H. Arakawa, *Sol. Energ. Mat. Sol. C* **2000**, *64*, 115.
- [197] J. J. Wu, G. R. Chen, H. H. Yang, C. H. Ku, J. Y. Lai, *Appl. Phys. Lett.* **2007**, *90*, 213109.
- [198] E. Hosono, S. Fujihara, T. Kimura, *Electrochim. Acta* **2004**, *49*, 2287.
- [199] W. J. Lee, A. Suzuki, K. Imaeda, H. Okada, A. Wakahara, A. Yoshida, *Jpn. J. Appl. Phys. Part 1* **2004**, *43*, 152.
- [200] M. K. I. Senevirathne, P. Pitigala, V. Sivakumar, P. V. Jayaweera, A. G. U. Perera, K. Tennakone, *J. Photochem. Photobiol. A* **2008**, *195*, 364.
- [201] R. J. Ellingson, M. C. Beard, J. C. Johnson, P. R. Yu, O. I. Micic, A. J. Nozik, A. Shabaev, A. L. Efros, *Nano Lett.* **2005**, *5*, 865.
- [202] V. I. Klimov, *J. Phys. Chem. B* **2006**, *110*, 16827.
- [203] G. Hodes, *J. Phys. Chem. C* **2008**, *112*, 17778.
- [204] A recent paper using CdS on TiO<sub>2</sub> nanotubes in a sulfide electrolyte reported a cell efficiency of 4.15%. W.-T. Sun, Y. Yu, H.-Y. Pan, X.-F. Gao, Q. Chen, L.-M. Peng, *J. Am. Chem. Soc.* **2008**, *130*, 1124. However, it has been demonstrated not to be a true conversion efficiency since the photovoltage was measured relative to the Ag/AgCl reference electrode rather than to the counter electrode in the sulfide electrolyte. The real cell efficiency would be ca. 1%. (Ref. [203]).
- [205] K. S. Leschkes, R. Divakar, J. Basu, E. Enache-Pommer, J. E. Boercker, C. B. Carter, U. R. Kortshagen, D. J. Norris, E. S. Aydil, *Nano Lett.* **2007**, *7*, 1793.
- [206] Y. Y. Tay, S. Li, F. Boey, Y. H. Cheng, M. H. Liang, *Physica B* **2007**, *394*, 372.
- [207] R. L. Puurunen, *Chem. Vap. Deposition* **2005**, *11*, 79.
- [208] H. Kumagai, M. Matsumoto, K. Toyoda, M. Obara, M. Suzuki, *Thin Solid Films* **1995**, *263*, 47.
- [209] M. Ritala, M. Leskela, L. Niinisto, P. Haussalo, *Chem. Mater.* **1993**, *5*, 1174.
- [210] A. Rahtu, M. Ritala, *Chem. Vap. Deposition* **2002**, *8*, 21.
- [211] M. Ritala, M. Leskela, E. Rauhala, *Chem. Mater.* **1994**, *6*, 556.

- [212] J. Aarik, J. Karlis, H. Mandar, T. Uustare, V. Sammelselg, *Appl. Surf. Sci.* **2001**, *181*, 339.
- [213] V. Pore, A. Rahtu, M. Leskela, M. Ritala, D. Sajavaara, J. Keinonen, *Chem. Vap. Deposition* **2004**, *10*, 143.
- [214] N. G. Park, J. van de Lagemaat, A. J. Frank, *J. Phys. Chem. B* **2000**, *104*, 8989.
- [215] H. B. Li, X. C. Duan, G. C. Liu, X. B. Jia, X. Q. Liu, *Mater. Lett.* **2008**, *62*, 4035.
- [216] Y. W. Wang, L. Z. Zhang, K. J. Deng, X. Y. Chen, Z. G. Zou, *J. Phys. Chem. C* **2007**, *111*, 2709.
- [217] S. H. Kim, Y. S. Cho, S. J. Jeon, T. H. Eun, G. R. Yi, S. M. Yang, *Adv. Mater.* **2008**, *20*, 3268.
- [218] G. R. Yi, V. N. Manoharan, E. Michel, M. T. Elsesser, S. M. Yang, D. J. Pine, *Adv. Mater.* **2004**, *16*, 1204.
- [219] Y. S. Cho, G. R. Yi, S. H. Kim, D. J. Pine, S. M. Yang, *Chem. Mater.* **2005**, *17*, 5006.
- [220] G. R. Yi, V. N. Manoharan, S. Klein, K. R. Brzezinska, D. J. Pine, F. F. Lange, S. M. Yang, *Adv. Mater.* **2002**, *14*, 1137.
- [221] S. H. Kim, S. Y. Lee, G. R. Yi, D. J. Pine, S. M. Yang, *J. Am. Chem. Soc.* **2006**, *128*, 10897.
- [222] G. K. Mor, O. K. Varghese, M. Paulose, K. Shankar, C. A. Grimes, *Sol. Energ. Mat. Sol. C* **2006**, *90*, 2011.
- [223] B. Tan, Y. Y. Wu, *J. Phys. Chem. B* **2006**, *110*, 15932.
- [224] T. Stergiopoulos, A. Ghicov, V. Likodimos, D. S. Tsoukleris, J. Kunze, P. Schmuki, P. Falaras, *Nanotechnology* **2008**, *19*, 235602.
- [225] J. H. Moon, G. R. Yi, S. M. Yang, D. J. Pine, S. Bin Park, *Adv. Mater.* **2004**, *16*, 605.
- [226] B. Erdem, E. D. Sudol, V. L. Dimonie, M. S. El-Aasser, *J. Polym. Sci. Part A* **2000**, *38*, 4441.
- [227] R. Rossmanith, C. K. Weiss, J. Geserick, N. Husing, U. Hormann, U. Kaiser, K. Landfester, *Chem. Mater.* **2008**, *20*, 5768.